Author/s:
O'Connell, B;Wallace, MW;Hood, AVS;Rebbechi, L;Brooks, HL

Title:
Deep water cuspate stromatolites of the Cryogenian Trezona Formation

Date:
2022-03-01

Citation:
O'Connell, B., Wallace, M. W., Hood, A. V. S., Rebbechi, L. & Brooks, H. L. (2022). Deep water cuspate stromatolites of the Cryogenian Trezona Formation. Geobiology, 20 (2), pp.194-215. https://doi.org/10.1111/gbi.12479.

Persistent Link:
https://hdl.handle.net/11343/299298

Deep-water cuspate stromatolites of the Cryogenian Trezona Formation

Brennan O'Connell[1], Malcolm W. Wallace[1],Ashleigh v.s. Hood[1], Luke Rebbecci[1], Hannah L. Brooks[1]

School of Earth Sciences, University of Melbourne, Parkville, Victoria 3051, Australia

Running head: deep-water cuspate stromatolites

Contact details for corresponding author: Brennan O'Connell: oconnellb@student.unimelb.edu.au and brennanoconnell2@gmail.com

ACKNOWLEDGMENTS

We thank Mark van Zuilen, Dawn Sumner, and two anonymous reviewers for constructive feedback that greatly improved the paper. We thank editors Kurt Konhauser and Mark van Zuilen for handling the paper. This study benefitted from discussion with Heidi Allen. Brennan O'Connell acknowledges funding from APPEA, AAPG, and IAS. Ashleigh Hood acknowledges funding from the Australian Research Council DECRA (DE190100988).

DR. BRENNAN O'CONNELL (Orcid ID : 0000-0002-5652-1222)
DR. ASHLEIGH HOOD (Orcid ID : 0000-0002-1430-2371)

Article type : Original Article

Deep water cuspate stromatolites of the Cryogenian Trezona Formation

Brennan O'Connell[1], Malcolm W. Wallace[1], Ashleigh v.s. Hood[1], Luke Rebbecci[1], Hannah L. Brooks[1]

[1]School of Earth Sciences, University of Melbourne, Parkville, Victoria 3051, Australia

Keywords: Neoproterozoic, stromatolite morphology, ocean redox, hardgrounds, deep water cycles, carbonate supersaturation, anoxia, Marinoan glacial cycles

ABSTRACT

Stromatolites and microbialites contain a rich repository of environmental and biological information. Despite extensive research, questions remain regarding the biological, chemical, and physical processes that control stromatolite macro, meso, and microstructure. We report unusual deep water cuspate stromatolites from the Cryogenian Trezona Formation, South Australia, from a mixed siliciclastic-carbonate open marine ramp setting. Cuspate stromatolite horizons develop near the base of decameter-scale transgression-regression cycles and typically overlie decimetre-scale irregular erosion surfaces. The cuspate structure within the stromatolites form near vertical, stacked cusp structures in cross section. In plan view, the cusps form cm-scale sharp parallel ridges oriented predominantly perpendicular to the regional down-slope direction and perpendicular to the elongation direction of stromatolites. We postulate that stromatolites colonised topographic highs of the irregular erosion surfaces (often hardgrounds) and grew in carbonate-supersaturated, iron rich marine waters in low turbidity sediment starved settings. Cuspate stromatolites are interpreted as forming during maximum transgression in condensed sections within deep water environments largely below storm wave base. Their microbial

metabolism may require low light and low oxygen. The deep water origin for the Trezona Formation cuspate stromatolites and other Precambrian cuspate stromatolites suggests a link between the cuspate morphology and physical/chemical(carbonate-supersaturated, low light, and low oxygen) conditions of Precambrian deep water marine settings.

INTRODUCTION

The Precambrian macroscopic fossil record is dominated by stromatolites that represent diverse and complex microbial communities (Grotzinger and Knoll, 1999). Stromatolites are a major feature of Proterozoic carbonate and mixed carbonate-siliciclastic systems (Grotzinger and James, 2000; Hoffman, 1974; Beukes, 1987) and are important indicators of paleoenvironment. The microstructure of stromatolites has been interpreted as being controlled by either biological (Walter, 1976; Bosak et al., 2012), or chemical processes (Grotzinger and Knoll, 1999; Visscher, Reid, and Bebout, 2000). Similarly, the controls on stromatolite macrostructure have been variably interpreted to be the result of either environmental (e.g., Golubic, 1976; Dill, Shinn, and Kendall 1989; Andres and Reid, 2006), or coupled environmental/biological processes (Ginsburg, 1991; Suosaari et al., 2019). Proposed factors include intrinsic biological controls of the microbial community, siliciclastic input, current energy, underlying substrate, light availability/depth of formation, geochemical conditions/redox gradients, degree of environmental-biological variability, and others (Walter, 1976; Horodyski, 1977a; Awramik and Vanyo, 1986; Ginsburg and Planavsky, 2008; Bosak et al., 2013; Mackey et al., 2017; and many others). Detailed sedimentological and petrographic observations of ancient stromatolites—considering the surrounding lithologies and association with cycles—can be used to shed light on the conditions that influence stromatolite occurrence and morphology.

In this study we report deep water cuspate stromatolites from the Cryogenian Trezona Formation in South Australia. We use the term ‘stromatolite’ to describe all laminated build-ups formed by sediment trapping, binding, and/or carbonate precipitation of microbes (as defined by Awramik, Margulis, and Barghoorn, 1976). The stromatolites described here form elongate domes with unusual cuspate laminations. They are developed in cyclic association with calcareous mudstone, hardgrounds, poorly sorted intraclastic packstone, and marine erosion surfaces in deep water settings. These deep water forms were likely deposited in low energy, low sedimentation, and carbonate supersaturated settings. These stromatolites add to a small

collection of deep water cuspate stromatolites. The deep water origin for the Trezona Formation stromatolites and other Precambrian cuspate stromatolites may suggest a link between Precambrian deep water settings (low light, low oxygen, carbonate supersaturated) and the cuspate morphology. There is an absence of similar cuspate stromatolites from the rock record after the Cryogenian with no known exact modern analogues of these forms. This may suggest the combined physical, biological, and geochemical conditions needed for deep water cuspate stromatolite growth did not exist after the Cryogenian.

GEOLOGICAL BACKGROUND

The Cryogenian Trezona Formation is part of the Upalinna Subgroup of the Umberatana Group, central Flinders Ranges of South Australia (Preiss, 2000; Fig. 1; Adelaide Fold Belt). The Upalinna Subgroup includes the upper nonglacial stratigraphy (late Cryogenian) between the Sturtian and Marinoan 'snowball Earth' glaciations (Fig. 2; Preiss, 1998). In the central Flinders Ranges, the Enorama Shale, Trezona, and Yaltipena formations (nonglacial strata, Fig. 2) underlie the Elatina Formation (Marinoan glacial sediment, Fig. 2) and thus record the "lead up" to the Marinoan glaciation. The Umberatana Group has few age constraints but includes U-Pb zircon dates from a tuffaceous horizon in the uppermost Sturtian diamictite with an age of 663.03 ± 0.11 Ma (Cox et al., 2018; Fig. 2), with no upper geochronologic constraints for the nonglacial sediment or Marinoan diamictite. In Tasmania, Australia, the termination of the Marinoan glaciation has been constrained to 636.41 ± 0.45 Ma, consistent with geochronological constraints that suggest the Marinoan glaciation ended ca. ~635 Ma globally (Calver et al., 2013; Rooney, Strauss, Brandon, and Macdonald, 2015). In Namibia, the Marinoan glaciation is constrained by the syn-glacial Ghaub Formation of Namibia with an age of 639.29 ± 0.26 Ma (U-Pb ID-TIMS) (Prave, Condon, Hoffmann, Tapster, and Fallick, 2016) and 635.5 ± 1.2 Ma (Hoffmann et al, 2004). In Death Valley, USA, the upper non-glacial Thorndike Submember is estimated at 651.69 ± 0.64 Ma (Nelson et al., 2020). In the Northern Flinders Ranges, the Balcanoona Formation (equivalent to the Etina Formation underlying the Trezona Formation; Fig. 2) is estimated to be ~650 Ma (Wallace et al., 2015). Therefore, based on available constraints and stratigraphic relationships, deposition of the Enorama Shale, Trezona, and Yaltipena formations is estimated to range in age from ~650 to 640 Ma.

The Trezona Formation has been the topic of considerable study, as it records one of the largest $\delta^{13}C$ excursions in Earth history, the 'Trezona Anomaly' (e.g., McKirdy et al., 2001; Ahm et al., 2021). Despite the importance of the Trezona Formation in understanding oceanic dissolved inorganic carbon leading up to 'snowball Earth', the sedimentology of the unit is not well understood. Although some authors have suggested a restricted or lacustrine origin for the Trezona Formation (Klaebe and Kennedy, 2019), the Trezona Formation is more commonly interpreted as marine—either a shallow low-energy lagoon (Preiss, 1987; Lemon, 1988) or open marine shelf to slope deposition (Rose et al., 2012).

METHODS and TERMINOLOGY

This study is focused on four locations in the central Flinders Ranges: Bulls Gap, Angorichina Hostel, Angorichina Station, and Glass Gorge Road (Fig. 1). Measured sections were taken ~5–20 km apart arranged proximal to distal, with one lateral/oblique (Figs. 1, 3). Stratigraphic sections were measured using a Jacob's staff at the centimetre and meter scale, noting bed thickness, lithology, sedimentary structures, and stromatolite morphology. Samples were collected within measured sections and in laterally equivalent beds for thin section analysis using transmitted light microscopy.

The terminology of Burchette and Wright (1992) is used to describe this mixed siliciclastic-carbonate ramp, whereby a ramp is defined as having a gentle slope which extends from the shoreline to the basin and is not rimmed nor is there a sharp distinct break in slope. The environments of a ramp setting are divided into inner, mid, and outer ramp environments. Ramp environments reflect deposition above fair weather wave base, between fair weather wave base and storm wave base, and below storm wave base, respectively. Cycle refers to a bounded package of repeated lithofacies with no implications for lateral continuity or a driving mechanism. Transgression, regression, and relative sea level change also do not suppose a driving mechanism (e.g., subsidence, eustacy, sediment supply).

Because of possible confusion/complications in describing mixed siliciclastic-carbonate lithologies, the terminology used in this paper is as follows: mudstone refers to a mix of silt and

clay with possible minor carbonate; calcareous mudstone refers to a mix of silt, clay, and carbonate. Intraclast refers to a clast of calcareous mudstone or micrite from the same basin (either eroded and redeposited in situ or eroded upslope and transported/deposited downslope); poorly-sorted intraclastic packstone refers to grain supported platy intraclasts with a fine-grained matrix (either micrite, mudstone, or calcareous mudstone, similar to "intraclastic breccia"); and rounded intraclastic packstone-grainstone refers to generally well-sorted grain-supported spherical and rod-like intraclasts with some fine-grained matrix (packstone) or no matrix (grainstone) present. The terms dolomitised mudstone/hardground refers to authigenic precipitation of dolomite on the seafloor (see Wallace et al., 2019); irregular marine erosion surface refers to a bedding surface with irregular erosional topography (up to ±1 m of relief over a few meters laterally along the bed). The terms ooid and giant ooid (instead of pisoid) refer to coated grains lacking obvious microbial textures.

STRATIGRAPHY and SEDIMENTOLOGY

The Trezona Formation conformably overlies the Enorama Shale (Preiss et al., 1987). The two units together make up a thick and laterally extensive shallowing upward succession (Rose et al., 2012) from deep water basinal mudstone, deep to shallow mixed siliciclastic-carbonate ramp facies, to shallow water carbonate ramp facies. The type section of the Trezona Formation is located at Enorama Creek and totals 240 m in thickness (Dalgarno and Johnson, 1964). Lemon (1988) noted that the lower and upper stratigraphy of the Trezona Formation is distinctly different in terms of lithology. Therefore, the Trezona Formation is informally divided into two members: a (lower and upper) siliciclastic member and a carbonate member (Table 1). The lower siliciclastic member consists of mudstone, interbedded mudstone and siltstone to very fine-grained sandstone, calcareous mudstone, intraclastic packstone, elongate cuspate stromatolites, erosion surfaces, and hardgrounds (these lithologies are the main focus of this study; Table 1). These lithologies transition upwards into the upper siliciclastic member. The upper siliciclastic member consists of mudstone to v.f.g sandstone, wavy, flaser, and lenticular bedded mixed lithologies, domal stromatolites, rare cuspate stromatolites, and crossbedded rounded intraclastic packstone-grainstone (Table 1). The siliciclastic member is in turn overlain by the carbonate member. The carbonate member consists of calcareous mudstone, micrite, ooid grainstone, rounded intraclastic grainstone, domal-columnar and longitudinal stromatolite

horizons, very rare cuspate stromatolites, and stromatolite bioherms (Table 1). The Trezona Formation is either overlain by the muddy tidal Yaltipena Formation (only present at the Bulls Gap locality in this study, Fig. 3) or unconformably overlain by the Marinoan glacial-associated sediment of the Elatina Formation (Angorichina Hostel, Glass Gorge, and Angorichina Station, Fig. 3; Priess, 1987).

Enorama Shale

The Enorama Shale is a poorly outcropping unit of green and red mudstone and siltstone at the base of the studied succession (Fig. 4; Table 1). Mudstone is finely laminated and can have a carbonate content of 12–30% (Preiss, 1987). These fine-grained lithologies form the valley units between the major carbonate units of the nonglacial Cryogenian sediments of the central Flinders Ranges (Figs. 1, 2). In the Blinman Region, the thickness of the Enorama Shale varies from 150–450 m (Preiss 1987). The Enorama Shale conformably underlies the Trezona Formation (Figs. 2, 3, 4A; Preiss, 1987). The basal third of the unit is dominated by red and red-brown siltstone, the middle third of the unit is dominated by laminated green mudstone with no coarse-grained beds, and the upper third of the unit is dominated by red siltstone and mudstone (Lemon, 1988). Red mudstone gradationally transitions into the overlying Trezona Formation. The Enorama Shale is documented in this study in the Angorichina Hostel, Angorichina Station, and Glass Gorge Road sections (Fig. 3).

In the Enorama Shale, silty sand and current ripple laminations in thin beds (10–30 cm) are occasionally present (Figs. 3,4). Some beds are sharp based with parallel lamination overlain by small-scale hummocky bedding (Fig. 4B; Lemon, 1988). At Angorichina Hostel and Glass Gorge, red siltstone and mudstone with sole marks are present and flutes indicate paleocurrent flow N–NW (Figs. 3, 4C). Other distinctive features include sharp-based or scoured beds with climbing ripples (Fig. 4D), and BCE Bouma divisions (Lemon, 1988). One bed with wave ripple cross lamination was noted north of the Glass Gorge section locality. Wave ripple features were not noted in any other localities. An unusual metre-scale red sand lense was noted at Angorichina Station.

Trezona Formation

The contact between the Enorama Shale and the Trezona Formation is placed at the first carbonate rich, poorly sorted intraclastic packstone and stromatolitic bed in the succession (Fig. 3). Measured sections of the Trezona Formation at Bulls Gap, Angorichina Hostel, Glass Gorge, and Angorichina Station are 90 to ~260 m thick (Fig. 3). The Trezona Formation is informally divided into two members in ascending order: a siliciclastic member (lower and upper) and a carbonate member (Table 1), described below.

Siliciclastic member

Lower siliciclastic member

The lower siliciclastic member is a mixed unit of fine-grained siliciclastic and carbonate sediment with a dominant siliciclastic component (Fig. 5; Table 1). Facies are non-cyclically and cyclically interbedded. Cycles in this unit are particularly well developed at the Glass Gorge locality (idealized in Fig. 6). At the base of each cycle is an erosion surface in calcareous mudstone with local topographic high and low points (Figs 5A,D, 6). This erosion surface has up to ± 1 metre of topographic variation in calcareous mudstone over a few meters laterally (Figs 5-A,D, 6). Topography on the erosion surface is difficult to measure with 2D exposures but appears to roughly parallel the paleocurrent direction and regional slope direction N–NW (Fig. 3). The erosion surface is overgrown by elongate cuspate stromatolites and rare columnar stromatolites (Fig. 5A, D), laterally associated with poorly-sorted intraclast packstone (Figs 5-A,D, 6). Stromatolites occupy the topographic highs of the marine erosion surface, while intraclastic packstone lithologies are generally found in the topographic lows of the marine erosion surface (Fig. 5D, 6). Stromatolitic laminae are finely cuspate (Fig. 5B, 6) and become progressively more clay-rich toward the uppermost layers.

The stromatolite beds are in turn overlain by recessively weathered gray-green to red-brown clay and mudstone (Fig. 5A, 6). Mudstone is generally finely laminated at the base, becoming progressively more resistant with interbedded silty and current rippled fine-grained sand beds upwards (Figs. 3, 6). Within the mudstone intervals, flute casts are preserved on the lower bed surfaces of coarser silty to very fine-grained sand beds, with paleocurrents generally oriented N-NW (regional down-slope directed). Current ripples in coarser beds similarly indicate dominant paleoflow N-NW. Purely siliciclastic lithologies are then overlain by interbedded calcareous

mudstone (often dolomitized or containing dolomitic nodules) and poorly-sorted intraclastic packstone (where the top few cm of the bed is often dolomitized). Intraclastic packstone beds are typically 10 to 40 cm thick with an erosional base (Figs. 5C, D, 6). Intraclasts are typically 5 mm–25 mm in length, with a mixture of iron oxide and carbonate lithologies. Angular elongate-platy intraclasts are generally poorly sorted with chaotic arrangement of clasts (Fig. 5C). In rare intraclast beds (generally not associated with stromatolites), imbricated and edgewise fabrics can be capped by hummocky cross stratified fine-grained carbonate grainstone. Interbedded, poorly-sorted elongate-platy intraclast packstone and calcareous mudstone beds are capped by an erosion surface that starts the next cycle. The erosion surface and underlying ~10 cm of stratigraphy may be dolomitized (Figs 5A, 6).

Upper siliciclastic member

The upper siliciclastic member is a mixed unit of fine-grained siliciclastic and carbonate sediment with a dominant siliciclastic component (Fig. 7; Table 1). The base of the upper siliciclastic member is arbitrarily placed where the following lithologies become common: crossbedded fine-grained grainstone; crossbedded well-sorted intraclastic packstone-grainstone; wavy, flaser, and lenticular bedded mixed lithologies; siltstone–fine-grained sandstone; and columnar and domal stromatolites without cuspate structures (Figs. 3, 7). Erosion surfaces and dolomitized beds rarely occur. Ooids are present, but rare. Well-sorted intraclastic packstone-grainstone beds are dominated by rounded intraclasts (40–95% rounded grains) (Fig. 7A). Rounded platy, rod-like, and spherical intraclastic equidimensional grains dominate, but there are also many complex and irregular shaped grains with angular irregular, internal cavities (Fig. 7A). Spherical grains are commonly <1 mm to 1 cm in diameter. Platy and rod-like grains are commonly <1mm to 3 cm. Outsized irregular intraclasts are up to 7 cm long. Intraclast beds tend to be thick (40 cm to 2 m) and commonly contain cross-lamination (several cm to ~30 cm thick) (Figs. 3, 7B). Most intraclasts consist of a mixture of iron oxides, micrite, and calcite (Fig. 7A). Micrite or blue-white marine cements commonly occupy the inter-intraclast space. Intraclastic packstone-grainstone and fine-grained grainstone can have mud drapes (Fig. 7C). Channelization and bidirectional currents in intraclast beds are common (Fig. 3). Wavy, flaser, and lenticular bedding are common in some intervals (Fig. 7E).

Cyclicity is also present in this unit (Fig. 7F). Domal (Fig. 7D) and rarer cuspate stromatolites directly overlie many lithology types: mudstone, erosional surfaces in mudstone (no hardground), crossbedded intraclast packstone-grainstone, and non-continuous erosionally-based crossbedded ooid packstone-grainstone (Fig. 3). Columnar stromatolites can also occur on the margins of crossbedded, channelised intraclast packstone-grainstone beds. Where present, cuspate stromatolites are poorly developed when compared with the underlying lower siliciclastic member. Similar to the underlying lower siliciclastic unit, stromatolites are overlain by clay and mudstone.

Carbonate member

The carbonate member is a mixed unit of siliciclastic and carbonate sediment dominated by carbonate lithologies (Fig. 8; Table 1). The base of the carbonate member is arbitrarily placed where carbonate strata become more prevalent, and mudstone units (found in the siliciclastic member) transition to more calcareous mudstone (up to 32% carbonate, Preiss, 1987) (Figs. 3, 8A; Table 1). Compared with the siliciclastic member, erosion surfaces are absent or less pronounced, there are only rare instances of dolomitized surfaces. Cuspate stromatolites are rare (see few occurrences at Angorichina Station, Fig. 3). At the base of the carbonate member, red-gray calcareous mudstone is interbedded with low relief stromatolites, longitudinal stromatolites (oriented N-NW), domal-columnar stromatolites, and intraclastic grainstone (Fig. 3; Fig. 8A-C). At the top of the carbonate member, this member becomes increasingly more massive and carbonate dominated (Figs 3, 8A). Calcareous mudstone can be desiccation-cracked (Fig. 8D). Thick, resistant massive blue-brown limestone beds of domal and columnar stromatolite bioherms can be up to 6 m thick (Fig. 8A). Oolitic grainstone is common (Fig 8 E,F) and is often associated with stromatolite bioherms (Fig. 3). Micritic ooids can have iron-oxide rich laminae. Ooids can be small (<1mm) to very large (giant ooids up to 2 cm, Fig. 8F). The uppermost resistant and thickest carbonate intervals of the Trezona Formation are ~28–60 m in thickness (Bulls Gap, Angorichina Station: Fig. 3, Fig. 8A).

Cuspate stromatolite occurrence, morphology, and petrology

279 Cuspate stromatolite horizons are commonly developed in cycles of the siliciclastic
280 member (Fig. 6). Biostromes of cuspate stromatolites in such cycles are laterally continuous and
281 can be traced for over 5 km. The stromatolite biostromes likely extend further, but the basin is
282 somewhat faulted with many offset beds and faulted intervals (Fig. 1). Elongate cuspate
283 stromatolites are found in all studied localities (Fig. 3). Cuspate stromatolites are best developed
284 at the base of the Trezona Formation in the lower siliciclastic member. Some cuspate intervals
285 are present in the upper siliciclastic member (Glass Gorge Road, Bulls Gap) and lower part of
286 the carbonate member (Angorichina Station, Fig. 3).
287 The cuspate stromatolites typically grow on an irregular erosion surface and hardground.
288 In almost all cases, irregular erosion surfaces develop over calcareous mudstone or mudstone
289 (Fig. 5A, 9A,B) and are associated with intraclast-rich lithologies. Along erosional horizons,
290 stromatolites develop on areas of high topography and intraclastic lithologies are found in
291 depressions on the erosional surface (Figs. 5D, 6). Lenses of intraclastic debris are occasionally
292 found in stromatolite depressions (gutters) along the biostrome. The erosion surface is commonly
293 dolomitized, and multiple erosion and dolomitization intervals are sometimes noted. The contact
294 between the stromatolite and underlying substrate is sharp. Elongate cuspate stromatolites
295 (described in detail, below) grade upwards into green or red-brown claystone and then mudstone
296 (Figs. 5A; 9 A,B). This upper contact is transitional: the cuspate stromatolite laminae become
297 progressively more clay-rich before stromatolites are overlain by clay and mudstone (Fig. 6)
298 At the macroscale, the stromatolite biostromes are ~tabular to irregular. The lower
299 surface is controlled by the irregular erosion surface and the upper surface is flat lying to gently
300 domed and continuous (Fig. 5A). The biostromes crop out conspicuously and are irregular along
301 strike (generally 0.5–1 m thick, Fig. 9). Cuspate stromatolites can be gently domed at the base
302 and be associated laterally with columnar stromatolites (where present) at the base of the
303 biostrome (Fig. 6). Gently domed elongate cuspate stromatolites and rarer columnar
304 stromatolites can transition upwards to continuous flatter-lying stratiform cuspate stromatolites.
305 Stromatolite growth is generally directed upwards and perpendicular to the underlying substrate.
306 In some cases, the associated columnar stromatolites grow in an inclined manner departing from
307 vertical growth.
308 Stromatolites are elongate at all localities (>0.60 m long, ~0.10 to 1 meter thick, ~0.10 to
309 ~2 m wide; Fig. 9A–C,G). In some localities, closely spaced cuspate stromatolites consist of only

one downslope elongate cuspate stromatolite over an erosion surface. These types are best developed at Bulls Gap, where cuspate stromatolites have irregular domed macrostructure (~4 m long, 50 cm thick, ~1m wide), with their long axis preferentially oriented NNW-SSE (SSE-oriented tail and a bulbus head- oriented NNW with and an average strike around 339° (n=11), Fig. 9G). Here, the morphology of the stromatolite domal macrostructure conforms to the underlying irregular erosion surface.

At the mesoscale, stromatolites are gently convex to stratiform structures with stacked, mm-scale cuspate laminae. Moving upwards, laminae appear to flatten as clay increases in stromatolite laminae. In cross section view, cusp peaks are vertically aligned, or slightly drift asymmetrically north (downslope; Fig. 5A and Fig. 9 E,F). In plan view, cuspate stromatolite peaks form straight or slightly sinuous cuspate ridges oriented perpendicular to the macroscale elongation direction of domes (see also Preiss, 1987) (Fig. 9 CD,G).

At the microscale, three main types of laminae are present in thin section: 1) dark micritic laminae forming cuspate ridges; 2) light micritic laminae with upward branching shrubby microbial textures; and 3) stylolitized red iron-oxide rich laminae (Fig. 10 A–D). There are distinct boundaries between all types of laminae. Dark micritic cuspate laminae and light micritic laminae form couplets (0.1–2 mm thick) (Fig. 10 A–B). Stylolitized dark red cuspate laminae are generally <0.2 mm in thickness and largely follow and accentuate the original cuspate lamination. Some stylolites also crosscut the original sedimentary lamination.

Dark micritic laminae form cuspate laminations and are made of homogeneous micrite, with minor siliciclastic and disseminated iron-oxide material (Fig. 10B). Upward tufted cuspate ridges can have a relief greater than 0.5 mm and are laterally linked by thinner, concave-up laminae (Fig. 10 A–C). Relief between the lowest and highest point along a single lamination is generally <1mm. Light micritic laminae with irregular upward branching shrubby microbial textures (Fig. 10D) appear to thicken between and drape over the dark micritic cuspate laminae to fill available space (Fig. 10B,D). Shrubby microbial types do not appear to construct the cusps. Microspar fills the intergranular space around irregular upward branching microbial textures (Fig. 10D). The cuspate laminae have a concave-upward profile on each side of the structure (Fig. 10B). Cuspate structures have low synoptic relief W>>H (Fig 10. A–C). The wavelength of the cusps generally ranges from around 6.5 mm to 8 mm. Cuspate features may be

linked vertically or can be disrupted by interstitial carbonates or stylolitized red iron-oxide rich laminae with no upward continuation. In gently convex cuspate stromatolites, dark micritic laminae are less cuspate and thin moving away from the top of the gently domed surface. Fine-grained iron oxides are disseminated in both the light micritic laminae and homogeneous dark micritic laminae (Fig. 10). Stylolitized red iron-oxide rich laminae concentrate very fine-grained iron oxides and clay. Fenestrae are not present. Voids are uncommon. Detrital grains like quartz are uncommon near the cusp ridges and become more common moving away from cuspate structures near the edge of the stromatolite.

Process interpretation and depositional setting of the Enorama and Trezona formations

The Enorama Shale is interpreted to represent deposition in a quiet, deep water environment (Preiss, 1987). The Enorama Shale shallows upward into outer ramp, middle ramp, and upper ramp mixed carbonate-siliciclastic environments of the Trezona Formation.

In the Enorama Shale, there are no mudcracks or indications of subaerial exposure. Siltstone beds with flute casts (Fig. 4C) and current ripple cross lamination are present but uncommon. These lithologies are likely deposited by dilute, low density turbidity currents, which suggests a distal location from sediment input source. Minor sharp-based parallel sandstone beds overlain by hummocky rippled beds are likely formed via oscillatory and combined flow during storm events (Dumas, et al., 2006).

The lower siliciclastic member of the Trezona Formation (Table 1) has thick accumulations of mudstone, silty beds with flute casts, calcareous mudstone (with dolomitic nodules), poorly-sorted platy-elongate intraclastic packstone, and irregular erosion surfaces. Thick accumulations of clay and mudstone are interpreted to represent deposition in a quiet, low energy deep water environment (similar to the underlying Enorama Shale). Thin siltstone beds with flute marks are interpreted as low density turbidites. Thin beds of erosively-based elongate-platy intraclast packstone likely represent debris flows deposited below fair weather wave base (Fig. 3). The platy-elongate and angular nature, chaotic arrangement of clasts, and poor sorting of the intraclasts indicate they were not subjected to extensive reworking, consistent with a mass flow origin. Rare occurrences of intraclasts with both imbricated and edgewise fabrics overlain by hummocky rippled very fine-grained grainstone—thought to require oscillatory and combined flow—may indicate some intraclast beds are storm event beds or debris flows reworked by

storms (Myrow et al., 2004). Elongate-platy intraclasts were likely sourced from a carbonate-rich environment or marine cemented beds up dip and were redeposited down dip.

Laterally continuous irregular erosion surfaces present below stromatolite layers (Fig. 5D), with as much as 1m of relief at an outcrop scale, are interpreted as deep water erosion surfaces. These may result from erosion during sediment starved conditions by deep water bottom currents or debris flow events on the ramp. Similar scale longitudinal bedforms and small furrows have been documented from deep water off the Bahama Outer Bank as a result of erosion by strong bottom currents (Hollister et al., 1974). Debris flows or strong bottom currents in deep water eroded down into partially lithified sediment to create the highly irregular topography. Topographic lows of the marine erosion surface are filled with intraclastic debris during mass flow events, or later infilled by downslope transport of intraclastic debris (erosion via filling of low areas may enhance topographic relief).

Dolomitized irregular erosion surfaces, dolomitized tops of some intraclastic packstone beds, and dolomitized mudstone beds are interpreted as hardgrounds associated with sediment starvation and authigenic dolomite precipitation, similar to other deep water hiatal surfaces in the Flinders Ranges (Wallace et al, 2019). Hardgrounds (hiatal surfaces) require long exposure to the seafloor under high carbonate saturation in sediment starved intervals, possibly linked with anoxia in Cryogenian deep marine settings (Wallace et al., 2019). Hardgrounds and associated cuspate stromatolites are interpreted to record deposition in deep water, low energy conditions completely below fair weather and largely below storm wave base in an outer to mid ramp setting (e.g., Burchette and Wright, 1992). Actual constraints on depth are difficult to estimate because there are many complexities in neritic and coastal settings, and wave base is a function of many factors such as wave height, fetch and period, sediment size, storm intensity (e.g., Immenhauser, 2009; Plint, James, and Dalrymple, 2010). Despite uncertainty, in modern shallow siliciclastic seas average fair weather wave base is ~10 ± 5 m and storm wave base is ~ 20 ± 5 m depth (Walker and Plint, 1992). We therefore place deposition of the lower siliciclastic member in at least ~10s to a couple 10s of meters depth. Such depths may be in the photic zone but in low light. For example, at 20 m depth in clear coastal water there is ~3% of surface irradiance (350–700 nm; Jerlov, 1976).

The upper siliciclastic member (Table 1) has laminated mudstone, domal-columnar stromatolites, heterolithic bedding, rounded intraclast packstone-grainstone, and fine-grained

grainstone. Spherical and rod-like rounded intraclast packstone-grainstone and fine-grained grainstone (Fig. 6 A,B,C) have large-scale crossbedding (Fig. 3). Less commonly, these lithologies have bidirectional crossbedding with mud drapes (Fig. 6C). Wavy, flaser and lenticular bedded mudstone-sandstone and limestone have variable paleocurrent indicators (no mudcracks) (Fig. 3; 6E). These higher energy lithologies suggest parts of the upper siliciclastic member were exposed to tidal, wave, and current reworking above fair weather wave base in subtidal conditions. Cycles with low and high energy lithologies are suggestive of deposition in a mid to inner mixed siliciclastic-carbonate ramp setting.

The carbonate member (Table 1) has calcareous mudstone, crossbedded ooids, grainstone, crossbedded rounded well-sorted intraclast grainstone, and massive domal-columnar stromatolite bioherms. The base of the carbonate member—with interbedded calcareous mudstone and a variety of stromatolite types—is similar to the upper siliciclastic member but more carbonate-rich (Fig. 8A). Calcareous mudstone and stromatolite lithologies may reflect low energy deposition in a carbonate rich mid to inner ramp setting. Moving upwards, the occurrence of ooid grainstone suggests continuous agitation of sediment in shallow, high energy conditions. Desiccation cracked calcareous mudstone beds are tidal flats (Fig. 8D). The carbonate member was influenced by tides and shallowed to intertidal conditions in rare instances (similar lithology to the overlying tidal Yaltipena Formation; Lemon, 1988). Massive crossbedded ooids, crossbedded rounded well-sorted intraclast grainstone, and massive domal-columnar stromatolite bioherms may represent deposition in the inner ramp setting, representing the culmination of the Enorama-Trezona shallowing upwards succession.

Palaeogeographically, the Bulls Gap section (south) is likely located more proximal to the shoreline than the Angorichina Hostel and Glass Gorge localities (north). This interpretation is based on the relative abundance of wave and current ripple cross lamination, more variable paleocurrents, more common and thicker crossbedded intraclastic grainstone, and coarser lithologies (Fig. 3; Bulls Gap). Evidence of deepening towards the north is consistent with the basin geometry suggested in previous studies (Preiss, 1987; Rose et al., 2012).

Our interpretation of a mixed siliciclastic-carbonate ramp for the Trezona Formation differs from earlier interpretations of a lagoonal-shallow marine system (Preiss et al., 1987; Lemon, 1988) or an isolated lacustrine basin (Klaebe and Kennedy, 2019). The restricted basin-lacustrine interpretation of Klaebe and Kennedy (2019) is not supported by our data, as evidence

for tidal currents during deposition of the Trezona Formation indicates a direct marine connection during deposition (Sztanó, 1995). Preiss et al. (1987) and Lemon (1988) noted the low-energy nature of the stromatolite beds and suggested a lagoonal (instead of deep water) setting. No barrier facies were noted in this study, and we suggest a deep water low energy origin for the stromatolites is supported by all available data.

Basin redox chemistry

The Trezona Formation has a variety of iron oxide rich lithologies, and they are strongly facies controlled. These include finely disseminated hematite in deep water cuspate stromatolite laminae, iron oxide rich intraclasts (up to 17% hematite; Preiss et al., 1987), and iron oxide rich ooids. The ooids have alternating carbonate and iron rich laminae (Fig. 8D). In all iron oxide rich lithologies, iron exists as very fine-grained hematite with no clear evidence for the replacement of ferrous precursor minerals. Such lithologies, and their strong facies/component control, suggest syn-sedimentary iron oxide precipitation within the Trezona Formation rather than later diagenetic iron enrichment. Syn-sedimentary iron oxide rich lithologies may provide clues to basin redox conditions during deposition. Iron oxide rich lithologies are present in all units of the Trezona Formation (from deep water to shallow water), suggesting iron oxidation in both shallow and subtidal conditions. This is consistent with other evidence for ferruginous ocean conditions and fluctuating redox conditions in this Cryogenian basin (Hood and Wallace, 2014; O'Connell et al., 2020) and elsewhere during the Cryogenian (Canfield, Poulton, Narbonne, 2007). We tentatively suggest a chemocline largely situated in deep water around the outer ramp setting. Iron oxide rich ooids also suggest incursions of anoxic marine water (delivering dissolved iron) into shallower environments of the basin.

Controls on cyclicity

The Trezona Formation is strongly cyclic (Fig. 7F). The repeating packages appear to reflect cyclic fluctuations in sediment delivery and sediment starvation. Such cyclic fluctuations may be allogenic related to subsidence or regression-transgression via eustatic or relative sea level change linked with sediment supply (Goodwin and Anderson, 1985; others). Alternatively, they may be autogenic and related to internal dynamics of the ramp system, or some combination of drivers.

Within the Enorama-Trezona shallowing upwards succession, cycles are highly regular (Fig. 7F), laterally extensive, and are often traceable over long distances (>5km along strike). Therefore, allogenic regression-transgression and associated changes in sediment supply likely play a role in deposition of cyclic packages. However, there can also be variability in stratigraphic thickness and lithology between cycles (Fig. 3), perhaps suggestive of a combination of drivers.

In the lower siliciclastic member, data suggest the erosion surface-hardground-stromatolite assemblage represents a condensed interval of sedimentation during maximum transgression of each transgression-regression cycle (Fig. 6). There are no shallow water lithologies or sedimentary structures associated with cuspate stromatolites. Association of cuspate stromatolites with poorly-sorted platy intraclastic packstone, marine erosion surfaces, and numerous hardgrounds (Fig. 6) is suggestive of sediment-starved conditions, elevated carbonate saturation, low energy (except for punctuated debris flow events), and prolonged exposure of the seafloor prior to and during stromatolite growth, consistent with a deep water origin. Carbonate saturation in this deep water setting may be linked with anoxia or low oxygen (Wallace et al., 2019). Intraclastic packstone lithologies are found in topographic lows on the erosion surface and occasionally as lenses in depressions (gutters) along the cuspate biostrome. This is unusual, as stromatolites associated with intraclasts are not typically associated with subtidal stromatolites (Kah et al., 2009). The association of stromatolites with poorly-sorted intraclastic packstone (large grain size) may seem, at first glance, hard to reconcile with an interpretation of stromatolite growth in deep water during maximum transgression. We suggest enhanced carbonate production during relative sea level rise resulted in increased carbonate sediment production and oversteepening of the ramp, resulting in instability and initiation of debris flows. This relationship has been demonstrated on modern carbonate platforms, where enhanced carbonate production during relative sea level rise increases mass wasting (Droxler and Schlager, 1985). In a somewhat analogous ancient setting, it is postulated that intraclast deposition resulted from widespread seafloor cementation and increased storm intensity during transgression, and thrombolites formed during max transgression in the absence of turbidity (Myrow et al., 2012). Some combination of factors is possible, whereby storms trigger mass flows on an unstable, oversteepened ramp. Following a large debris flow, deep water conditions would be extremely sediment starved with conditions suitable for cuspate stromatolite growth.

Transgression-regression cycles occur against a large-scale backdrop of relative sea level fall during the Enorama-Trezona shallowing upward succession. What was the driver of relative sea level fluctuations? Syn-sedimentary diapir movement has been suggested as a relative sea level control during deposition of the Trezona Formation (Lemon, 1988; Klaebe and Kennedy, 2019). Syn-sedimentary diapir movement may have caused some variability in stratigraphic thickness, relative depth, and lithology between sites. Another driver may be eustatic changes in sea level, linked with sediment supply. Cycles in coeval strata in the Yukon have been interpreted as cyclic deepening and shallowing during the lead up to the Marinoan glaciation (Day et al., 2004). Given the Trezona cycles are highly regular and do closely precede the Marinoan glaciation, we speculate that the cycles may be tied to eustatic fluctuations caused by the buildup and decay of ice sheets in high latitude regions. In this sense, the Trezona cycles may record the beginnings of the global Marinoan glaciation.

Broadly, evidence for condensed stromatolite deposition during maximum transgression of cycle may suggest the need for careful consideration and independent evidence for paleoenvironmental conditions when interpreting stromatolites in ancient mixed siliciclastic-carbonate settings. Carbonate-rich lithologies and stromatolites are commonly interpreted as shallow water intervals during cyclic sedimentation. This may not always apply to mixed settings or deep water cycles (Myrow et al., 2012; this study), especially considering carbonate saturation at depth during the Precambrian (Wallace et al., 2019).

Factors influencing the occurrence and morphology of cuspate stromatolites

The distinctive cuspate morphology of the stromatolites of the base of the siliciclastic member (and their elongate macrostructure) is not typical of the stromatolites from the shallower-water carbonate member of the Trezona Formation. The environmental factors relating to stromatolite occurrence and growth are largely interpreted as the result of transgression-regression cycles in deep water (discussed above). Stromatolite growth appears to be linked with sediment starvation and associated elevated carbonate saturation. Other controlling factors include a hard underlying substrate (hardground formation), topography on irregular marine erosion surfaces, and downslope-oriented currents.

Stromatolites are here interpreted as growing in sediment starved conditions during maximum transgression. A resumption of sediment supply and increase in clay delivery at the

top of stromatolite biostromes eventually leads to their demise (Fig. 6). Sediment flux also appears to influence stromatolites morphology at the mesostructure scale. Overlying the erosion surface, stromatolites form elongate domes with cuspate laminae. Moving upwards, laminae appear to flatten as clay increases in stromatolite laminae. Other studies have similarly noted a flattening of stromatolite laminae corresponding with increased sediment flux (Mackey et al., 2017).

Based on the stromatolite morphology, carbonate composition, condensed nature, and association with hardgrounds, another factor that appears to control stromatolite growth and occurrence is elevated carbonate saturation. Although they contain some detrital material (iron oxides and quartz), stromatolites are dominantly composed of micrite with delicate cuspate and upward branching shrubby microbial textures. The micritic composition and preservation of delicate microbial features is most consistent with direct carbonate precipitation by stromatolite-forming microbial communities. Carbonate saturation may be linked with low sediment flux and anoxia in Precambrian deep water settings (Wallace et al., 2019), explaining why cuspate stromatolites are best developed at the base of the section (deepest water). The association of stromatolites overlying hardgrounds may also suggest stromatolites preferred to colonise hard substrates. A hard substrate, however, may not be strictly necessary as there are a few instances of cuspate stromatolite growth on top of poorly cemented mudstone moving up-section.

Stromatolites colonised the topographic highs of the erosion surface and are laterally associated with elongate-platy intraclastic packstone in topographic lows. This may indicate stromatolites preferred to grow in less turbulent conditions. Both the underlying erosion surface and downslope currents appear to have a control on the elongation morphology. At Bulls Gap, stromatolite bioherm domes are oriented ~N-NW, roughly parallel to both the downslope slope direction and the predominant paleo-current direction (Fig. 3). Their morphology with a S-SE tail and a bulbous nose N-NW (downslope) (Fig. 9G) is also likely current controlled.

Individual cusps can be slightly asymmetrical leaning N-NW, possibly caused by cuspate growth structures drifting downslope under current flow. Straight-sinuous ridges are oriented perpendicular to stromatolite elongation (in plan view). Because the parallel-slightly sinuous ridges are present on stromatolites (precipitated carbonate instead of detrital sediment), have a high angle of repose, short wavelength, and are linked with individual cusps, they are interpreted

as growth structures. However, their parallel-slightly sinuous ridge growth morphology may be somewhat influenced by microorganism interaction with currents.

At the microscale, the interaction of at least two different microorganism communities (cuspate and upward branching shrubby lamina types) likely control the unusual morphology of deep water cuspate stromatolites. Low synoptic relief of cuspate ridges may be the result of similar growth rates for cuspate and upward branching shrubby lamina types. Shrubby microbes commonly drape over cuspate ridges and thicken in the inter-cusp space, filling available accommodation. Cuspate microorganisms must continuously re-establish on the stromatolite surface, which may prevent them from gaining high synoptic relief. It is also possible that low synoptic relief of cusps is a biological feature. The gently domed morphology (when not controlled by the underlying erosion surface) appears to reflect thickening and preferential growth of microorganism types in the middle of the dome. Dark micritic laminae are less cuspate and thin moving away from the top of the gently domed surface. Therefore, upward branching shrubby microbes do not have an elevated cuspate surface to continuously drape over at the edge of the gently domed structure.

Comparison with other Precambrian cuspate stromatolites

Stromatolites and fenestrate microbialites with a cuspate morphology have been documented from several Archean and Proterozoic successions (Fig. 11; Hoffman, 1974; Beukes, 1987; Sumner, 1997; Flannery and Walter, 2012; Bartley et al., 2015; Kurucz and Fralick, 2018). Similar morphologies have been variously referred to as Thyssagetacean-type stromatolites (Vlasov, 1977, in Hofman and Masson, 1994), thesaurus stromatolites (Hofmann and Masson, 1994), peak or peak-shaped stromatolites (Jackson, 1989), or tufted microbialites (Flannery and Walter, 2012). In addition, cuspate stromatolites share some similarities with coniform stromatolites and cuspate/tented fenestrate microbialites (Sumner 1997).

In the Mesoproterozoic Dismal Lakes Group, cuspate stromatolites formed offshore in a sediment-starved outer platform setting, with a minimum depth for cuspate growth of 12 m, but perhaps up to ~80 meters depth in low oxygen carbonate supersaturated settings below wave base (Bartley et al., 2015). Bartley et al. (2015) interpreted the vertical and horizontal components as a result of the interplay of different microbial communities, potentially driven by light availability or variable redox conditions. Although the environment of deposition and

cuspate morphology is grossly similar, strong vertical supports, pyrite laminae, and substantial primary void space are present in the Dismal Lakes stromatolites (Bartley et al., 2015), unlike the Trezona cuspate stromatolites. It's not clear if the Dismal Lakes Group cuspate stromatolites have linked ridges on the top of the structure (Bartley et al., 2015, but see their Fig. 10). In the Gamohaan and Frisco formations of the Campbellrand Subgroup, South Africa, cuspate fenestrate microbialites have also been interpreted as being of deep subtidal origin (Sumner, 1997). These fenestrate microbialites are characterized by a netlike framework of fine, dark carbonate laminae, cemented by fibrous calcite, which form stacked true cuspate microstructures (but lack iron oxides and parallel cusp ridges in plan view). Cuspate microbialites of the Pethei Group are interbedded with turbidites and basin-slope facies and are also interpreted as deep water forms (Fig. 11B; Hoffman, 1974). Perhaps most similar to the Trezona Formation stromatolites are the elongated Boetsap-style giant stromatolite mounds with red tufted laminations in the Archean Campbellrand Subgroup (Beukes, 1987; Fig. 11C). Their cuspate morphology is similar, and the downslope elongation of domes is also similar to the Trezona Formation cuspate stromatolites. The Boetsap cuspate structures also appear to have Trezona-style parallel-slightly sinuous ridges (Alexander, 2020). The elongated mounds at Boetsap have been interpreted as subtidal (Truswell and Eriksson, 1973; Beukes, 1987), but it's not known how deep. Similar cuspate stromatolites have also been found in the Neoproterozoic Callison Lake Formation in the Yukon, Canada (Fig. 11D; Strauss et al., 2015). They are associated with low energy lithologies in likely deep water. Callison Lake Formation cuspate stromatolites are not associated with iron oxides.

Precambrian cuspate stromatolites share a similar subtidal deep water origin (Hoffman, 1974; Sumner, 2007; Bartley et al., 2015). In at least one case, cuspate stromatolites were also interpreted as being formed in carbonate supersaturated, sediment starved, and low oxygen settings (Bartley et al., 2015). Other insights, such as environmental/sedimentological setting, redox setting (low oxygen, ferruginous, euxinic), low light, carbonate supersaturated, etc were not able to be gleaned from existing work on cuspate stromatolites. The deep water origin of the Trezona Formation cuspate stromatolites and most other Precambrian cuspate stromatolites may suggest: 1) cuspate stromatolites may be deep water indicators if supported by the associated lithologies; and 2) there may be a link between the cuspate morphology and the biological, physical, and chemical conditions of Precambrian deep water marine settings.

Modern cuspate microbialties

Modern cuspate forms include mineralised pinnacle cuspate and tufted structures found in Antarctic sub-glacial lakes (Parker et al., 1981; Sumner et al., 2016; Mackey et al., 2017), unmineralized forms in sabkha and salt marsh environments of the Laguna Figueroa, Baja California, Mexico (Horodyski and Bloeser, 1977b), and cuspate mat forms in Shark Bay (Awramik and Vanyo, 1986; Flannery and Walter, 2012). Some cuspate features, although documented from different environments, share a continuously submerged, low energy, low turbulence, and low sedimentation setting (Horodyski and Bloeser, 1977; Parker et al., 1981; Mackey et al., 2017). These environmental variables are similar to the Trezona Formation cuspate stromatolites.

Despite some similarities, modern cuspate forms are not robust analogues for the deep water cuspate stromatolites of the Trezona Formation. Modern examples tend to be characterized by isolated tufts/cusps/pinnacles (Parker, 1981; Horodyski and Bloeser, 1977; Sumner et al., 2016) or cusps that have a reticulate, net-like geometry (Flannery and Walter, 2012). Ridges in microbial mats can be oriented perpendicular to tidal currents in the Lyngbya mats of Shark Bay (Awramik and Vanyo, 1986; their Fig. 2B). However, their microstructure is not similar, as tufts are non-laminar with grains and patchy micrite in thin section (Jahnert and Collins, 2013). In contrast to modern examples, in the Trezona Formation each laminated cusp (in cross section view) makes up a straight or slightly sinuous ridge (in plan view) that is perpendicular to the downslope elongation direction of the stromatolite and downslope oriented currents (Fig. 9D). To our knowledge, no similar cuspate forms have been documented in the modern. This difference in mat structure potentially means that modern tufted forms may be only partially related or perhaps even completely unrelated to the Trezona Formation cuspate forms. Some similarities in mat structure may not reflect a true homology.

To our knowledge, no cuspate stromatolites similar to the cuspate stromatolites of the Trezona Formation have been documented after the Cryogenian. For example, Late Devonian deep water stromatolites have a large variety of morphologies, but no cuspate structures (Playford, Hocking, Cockbain, 2009). It may be possible that cuspate deep water forms are linked to specific biological, chemical, and physical processes (low light, low oxygen, carbonate

supersaturated, and/or possibly fluctuating redox conditions) in Precambrian deep water settings that did not persist after the Cryogenian.

Possible cuspate stromatolite metabolism

Deciphering the metabolism of ancient stromatolites is problematic, but some constraints can be placed on the cuspate forms described here. It is unlikely that the Trezona cuspate microorganisms had sulphur-based metabolisms, as neither sulphide minerals (such as pyrite) nor their weathered pseudomorphs are present in the cuspate stromatolite laminae. While there is finely disseminated hematite in the stromatolite laminae, it is unlikely that the Trezona cuspate forms were constructed by chemotropic iron-oxidizing microorganisms. The apices of some cusps do show high concentrations of iron oxide (Fig 10A,C). However, iron oxide is not generally concentrated in specific lamina types, as would be expected for microbially-mediated iron precipitation (Planavsky et al., 2009). Finely disseminated hematite is also present throughout the Trezona Formation and is not restricted to the cuspate stromatolites. There are also no iron oxides associated with similar deep water cuspate stromatolites in the Callison Lake Formation (Fig. 11D). Therefore, there is little evidence to support a dominant role for iron-oxidizing microbes in the formation of cuspate stromatolites.

Cuspate stromatolites in the Trezona Formation grew in deep water settings, perhaps suggestive of a microbial metabolism that could persist in low light settings or may have even been independent of photosynthesis. The mesoscale structure of Trezona cuspate stromatolites have a gently domed convex morphology. This morphology is commonly linked with a phototrophic growth response, which may be suggestive of low light dependence (e.g., Awramik and Vanyo, 1986; however, see Petryshyn and Corsetti, 2011).

Cuspate stromatolites appear to span the rock record from the Archean through to the Cryogenian mid Neoproterozoic. Cuspate stromatolites are not present after the Cryogenian. This may reflect a relationship with anoxia—their disappearance perhaps related to Neoproterozoic oxygenation. Some research indicates that the Ediacaran late Neoproterozoic is characterized by increasing levels of oxygenation (Fike et al., 2006 and many others). Cuspate stromatolites may have required a very specific set of conditions such as a combination of low light (as their deep-water occurrence would suggest) and anoxia. After the Cryogenian, the oxic/anoxic chemocline may have been too deep to support both low light and anoxia. Hence this ecological niche may

have been completely removed from the Earth and Trezona-style cuspate stromatolites became extinct.

CONCLUSIONS

Unusual cuspate stromatolites in the Trezona Formation are interpreted as forming during maximum transgression as condensed sections in deep water settings. Stromatolite occurrence and morphology is related to cyclic processes on the marine shelf (transgression-regression and associated sediment supply, debris flows), chemical processes (carbonate supersaturation and low oxygen), hardground formation, sediment starvation/siliciclastic influx, topography on irregular marine erosion surfaces, and downslope oriented currents. Cuspate stromatolites growth during maximum transgression in deep water cycles suggests the need for careful evaluation and independent evidence of paleoenvironmental conditions (relatively deep versus shallow) when interpreting mixed siliciclastic-carbonate cyclic sedimentation. The deep water origin for the Trezona Formation cuspate stromatolites and other Precambrian cuspate stromatolites may suggest: 1) cuspate stromatolites are deep water indicators if supported by the associated lithologies; and, 2) there may be a link between the cuspate morphology and the biological, physical, and chemical conditions of Precambrian deep marine settings. After the Cryogenian, the chemocline may have been too deep to support both low light and low oxygen cuspate forming microbial metabolisms.

ACKNOWLEDGMENTS

We thank Mark van Zuilen, Dawn Sumner, and two anonymous reviewers for constructive feedback that greatly improved the paper. We thank editors Kurt Konhauser and Mark van Zuilen for handling the paper. This study benefitted from discussion with Heidi Allen. Brennan O'Connell acknowledges funding from APPEA, AAPG, and IAS. Ashleigh Hood acknowledges funding from the Australian Research Council DECRA (DE190100988).

REFERENCES

Ahm, A.-S. C., Bjerrum, C. J., Hoffman, P. F., Macdonald, F. A., Maloof, A. C., Rose, C. V., . . . Higgins, J. A. (2021). The Ca and Mg isotope record of the Cryogenian Trezona carbon isotope excursion. Earth and Planetary Science Letters, 568, 117002.

Alexander, J. H. (2020). Patterns within centimeter-scale bedding in carbonate rocks in the Archean Transvaal Supergroup, South Africa.

Andres, M. S., & Reid, R. P. (2006). Growth morphologies of modern marine stromatolites: a case study from Highborne Cay, Bahamas. Sedimentary Geology, 185(3-4), 319-328.

Awramik, S., Margulis, L., & Barghoorn, E. (1976). Evolutionary processes in the formation of stromatolites. In Developments in Sedimentology (Vol. 20, pp. 149-162): Elsevier.

Awramik, S. M., & Vanyo, J. P. (1986). Heliotropism in modern stromatolites. Science, 231(4743), 1279-1281.

Bartley, J., Kah, L., Frank, T., & Lyons, T. (2015). Deep-water microbialites of the Mesoproterozoic Dismal Lakes Group: microbial growth, lithification, and implications for coniform stromatolites. Geobiology, 13(1), 15-32.

Beukes, N. J. (1987). Facies relations, depositional environments and diagenesis in a major early Proterozoic stromatolitic carbonate platform to basinal sequence, Campbellrand Subgroup, Transvaal Supergroup, Southern Africa. Sedimentary Geology, 54(1-2), 1-46.

Bosak, T., Knoll, A. H., & Petroff, A. P. (2013). The meaning of stromatolites. Annual Review of Earth and Planetary Sciences, 41, 21-44.

Bosak, T., Liang, B., Wu, T. D., Templer, S., Evans, A., Vali, H., . . . Mui, J. (2012). Cyanobacterial diversity and activity in modern conical microbialites. Geobiology, 10(5), 384-401.

739
740 Burchette, T. P., & Wright, V. P. (1992). Carbonate ramp depositional systems. Sedimentary
741 Geology, 79(1), 3-57. doi:http://dx.doi.org/10.1016/0037-0738(92)90003-A
742
743 Calver, C., Crowley, J., Wingate, M., Evans, D., Raub, T., & Schmitz, M. (2013). Globally
744 synchronous Marinoan deglaciation indicated by U-Pb geochronology of the Cottons Breccia,
745 Tasmania, Australia. Geology, 41(10), 1127-1130.
746
747 Canfield, D. E., Poulton, S. W., & Narbonne, G. M. (2007). Late-Neoproterozoic deep-ocean
748 oxygenation and the rise of animal life. Science, 315(5808), 92-95.
749
750 Cox, G. M., Isakson, V., Hoffman, P. F., Gernon, T. M., Schmitz, M. D., Shahin, S., . . .
751 Nordsvan, A. (2018). South Australian U-Pb zircon (CA-ID-TIMS) age supports globally
752 synchronous Sturtian deglaciation. Precambrian Research, 315, 257-263.
753 doi:10.1016/j.precamres.2018.07.007
754
755 Dalgarno, C.R., Johnson, J.E., 1964. The Wilpena Group. In Thomson et al., Precambrian Rock
756 Groups in the Adelaide Geosyncline: A new subdivision. Quarterly Geological Notes,
757 Geological Survey of South Australia, 9, 1–19.
758
759 Day, E. S., James, N. P., Narbonne, G. M., & Dalrymple, R. (2004). A sedimentary prelude to
760 Marinoan glaciation, Cryogenian (Middle Neoproterozoic) Keele Formation, Mackenzie
761 Mountains, northwestern Canada. Precambrian Research, 133(3-4), 223-247.
762
763 Dill, R. F., Shinn, E. A., & Kendall, C. G. S. C. (1989). Giant Subtidal Stromatolites and Related
764 Sedimentary Features: Lee Stocking Island, Exumas, Bahamas, July 20-22 American
765 Geophysical Union, Field Trip Guidebook T373, 33 p. American Geophysical Union.
766
767 Droxler, A. W., & Schlager, W. (1985). Glacial versus interglacial sedimentation rates and
768 turbidite frequency in the Bahamas. Geology, 13(11), 799-802.
769

770 Dumas, S., & Arnott, R. (2006). Origin of hummocky and swaley cross-stratification—The
771 controlling influence of unidirectional current strength and aggradation rate. Geology, 34(12),
772 1073-1076.
773
774 Fike, D.A., Grotzinger, J.P., Pratt, L.M. & Summons, R.E. (2006). Oxidation of the Ediacaran
775 ocean. Nature, 444, 744-747.
776
777 Flannery, D. T., & Walter, M. R. (2012). Archean tufted microbial mats and the Great Oxidation
778 Event: new insights into an ancient problem. Australian Journal of Earth Sciences, 59(1), 1-11.
779
780 Ginsburg, R. (1991). Controversies about stromatolites: vices and virtues. In: Controversies in
781 Modern Geology: Evolution of Geological Theories in Sedimentology, Earth History and
782 Tectonics (Ed. By D.W Müller, J. A. McKenzie and H Weissert), pp. 25-36. Academic Press,
783 London.
784
785 Ginsburg, R. N., & Planavsky, N. J. (2008). Diversity of Bahamian microbialite substrates. In
786 Links Between Geological Processes, Microbial Activities&Evolution of Life (pp. 177-195):
787 Springer.
788
789 Golubic, S. (1976). Organisms that build stromatolites. In Developments in Sedimentology (Vol.
790 20, pp. 113-126): Elsevier.
791
792 Goodwin, P. W., & Anderson, E. (1985). Punctuated aggradational cycles: a general hypothesis
793 of episodic stratigraphic accumulation. The Journal of Geology, 93(5), 515-533.
794
795 Grotzinger, J. P., & James, N. P. (2000). Precambrian carbonates: evolution of understanding.
796
797 Grotzinger, J. P., & Knoll, A. H. (1999). Stromatolites in Precambrian carbonates: evolutionary
798 mileposts or environmental dipsticks? Annual Review of Earth and Planetary Sciences, 27(1),
799 313-358.
800

801 Hoffman, P. (1974). Shallow and deep-water stromatolites in Lower Proterozoic platform–to–
802 basin facies change, Great Slave Lake, Canada. AAPG Bulletin, 58(5), 856-867.
803
804 Hoffmann, K.-H., Condon, D., Bowring, S., & Crowley, J. (2004). U-Pb zircon date from the
805 Neoproterozoic Ghaub Formation, Namibia: constraints on Marinoan glaciation. Geology, 32(9),
806 817-820.
807
808 Hofmann, H. J., & Masson, M. (1994). Archean stromatolites from Abitibi greenstone belt,
809 Quebec, Canada. Geological Society of America Bulletin, 106(3), 424-429.
810
811 Hollister, C. D., Flood, R. D., Johnson, D. A., Lonsdale, P., & Southard, J. B. (1974). Abyssal
812 furrows and hyperbolic echo traces on the Bahama Outer Ridge. Geology, 2(8), 395-400.
813
814 Hood, A. V., & Wallace, M. W. (2014). Marine cements reveal the structure of an anoxic,
815 ferruginous Neoproterozoic ocean. Journal of the Geological Society, 171(6), 741-744.
816
817 Hood, A. V., & Wallace, M. W. (2012). Synsedimentary diagenesis in a Cryogenian reef
818 complex: Ubiquitous marine dolomite precipitation. Sedimentary Geology, 255, 56-71.
819
820 Horodyski, R. J. (1977a). Environmental influences on columnar stromatolite branching patterns:
821 examples from the Middle Proterozoic Belt Supergroup, Glacier National Park, Montana. Journal
822 of Paleontology, 661-671.
823
824 Horodyski, R. J., & Bloeser, B. (1977b). Laminated algal mats from a coastal lagoon, Laguna
825 Mormona, Baja California, Mexico. Journal of Sedimentary Research, 47(2), 680-696.
826
827 Immenhauser, A. (2009). Estimating palaeo-water depth from the physical rock record. Earth-
828 Science Reviews, 96(1-2), 107-139.
829

Jackson MJ (1989) Lower Proterozoic Cowles Lake foredeep reef, N.W.T., Canada. In: Geldsetzer HHJ, James NP, Tebbutt GE (eds), Reefs, Canada and adjacent area. Canadian Society of Petroleum Geologists, Memoir 13: 64–71.

Jahnert, R. J., & Collins, L. B. (2013). Controls on microbial activity and tidal flat evolution in Shark Bay, Western Australia. Sedimentology, 60(4), 1071-1099.

Kah, L. C., Bartley, J. K., Stagner, A. F., Swart, P., Eberli, G., McKenzie, J., . . . Stevens, T. (2009). Reinterpreting a proterozoic enigma: Conophyton–Jacutophyton stromatolites of the Mesoproterozoic Atar group, Mauritania (Vol. 41): John Wiley and Sons, Ltd Chichester, West Sussex, UK.

Klaebe, R., & Kennedy, M. (2019). The palaeoenvironmental context of the Trezona anomaly in South Australia: Do carbon isotope values record a global or regional signal? The Depositional Record, 5(1), 131-146.

Kurucz, S., & Fralick, P. (2018). Internal fabric of giant domes in the Mesoarchean Steep Rock carbonate platform, Superior Province, Canada. Canadian Journal of Earth Sciences, 55(4), 343-355.

Lemon, N. M. (1988). Diapir recognition and modelling with examples from the late Proterozoic Adelaide Geosyncline, central Flinders Ranges, South Australia.

Mackey, T. J., Sumner, D. Y., Hawes, I., Jungblut, A. D., Lawrence, J., Leidman, S., & Allen, B. (2017). Increased mud deposition reduces stromatolite complexity. Geology, 45(7), 663-666.

McKirdy, D. M., Burgess, J. M., Lemon, N. M., Yu, X., Cooper, A. M., Gostin, V. A., . . . Both, R. A. (2001). A chemostratigraphic overview of the late Cryogenian interglacial sequence in the Adelaide Fold-Thrust Belt, South Australia. Precambrian Research, 106(1-2), 149-186.

Myrow, P. M., Taylor, J. F., Runkel, A. C., & Ripperdan, R. L. (2012). Mixed siliciclastic–carbonate upward-deepening cycles of the Upper Cambrian inner detrital belt of Laurentia. Journal of Sedimentary Research, 82(4), 216-231.

Myrow, P. M., Tice, L., Archuleta, B., Clark, B., Taylor, J. F., & Ripperdan, R. L. (2004). Flat-pebble conglomerate: its multiple origins and relationship to metre-scale depositional cycles. Sedimentology, 51(5), 973-996.

Nelson, L. L., Smith, E. F., Hodgin, E. B., Crowley, J. L., Schmitz, M. D., & Macdonald, F. A. (2020). Geochronological constraints on Neoproterozoic rifting and onset of the Marinoan glaciation from the Kingston Peak Formation in Death Valley, California (USA). Geology, 48(11), 1083-1087.

O'Connell, B., Wallace, M. W., Hood, AvS., Lechte, M. A., & Planavsky, N. J. (2020). Iron-rich carbonate tidal deposits, Angepena Formation, South Australia: A redox-stratified Cryogenian basin. Precambrian Research, 342, 105668.

Parker, B. C., Simmons Jr, G. M., Love, F. G., Wharton Jr, R. A., & Seaburg, K. G. (1981). Modern stromatolites in Antarctic dry valley lakes. BioScience, 31(9), 656-661.

Petroff, A. P., Sim, M. S., Maslov, A., Krupenin, M., Rothman, D. H., & Bosak, T. (2010). Biophysical basis for the geometry of conical stromatolites. Proceedings of the National Academy of Sciences, 107(22), 9956-9961.

Petryshyn, V., & Corsetti, F. (2011). Analysis of growth directions of columnar stromatolites from Walker Lake, western Nevada. Geobiology, 9(5), 425-435.

Planavsky, N., Rouxel, O., Bekker, A., Shapiro, R., Fralick, P., & Knudsen, A. (2009). Iron-oxidizing microbial ecosystems thrived in late Paleoproterozoic redox-stratified oceans. Earth and Planetary Science Letters, 286(1-2), 230-242.

Playford, P., Hocking, R., & Cockbain, A. (2009). Devonian reef complexes of the Canning Basin, Western Australia. Geological Survey of Western Australia. Bulletin 145. Perth, WA, Australia: Western Australian Museum.1-444.

Plint, A., James, N., & Dalrymple, R. (2010). Wave-and storm-dominated shoreline and shallow-marine systems. Facies models, 4, 167-200.

Prave, A. R., Condon, D. J., Hoffmann, K. H., Tapster, S., & Fallick, A. E. (2016). Duration and nature of the end-Cryogenian (Marinoan) glaciation. Geology, 44(8), 631-634.

Preiss, W. (2000). The Adelaide Geosyncline of South Australia and its significance in Neoproterozoic continental reconstruction. Precambrian Research, 100(1-3), 21-63.

Preiss, W. V. (1987). The Adelaide Geosyncline: Late Proterozoic stratigraphy, sedimentation, palaeontology and tectonics: Department of Mines and Energy. 1-438

Preiss, W. V., Dyson, I. A., Reid, P., & Cowley, W. (1998). Revision of lithostratigraphic classification of the Umberatana Group. Mesa Journal, 9, 36-42.

Reid, P., & Preiss, W. (1999). Parachilna map sheet. Geological Survey of South Australia Atlas, 1(250), 000.

Rooney, A. D., Strauss, J. V., Brandon, A. D., & Macdonald, F. A. (2015). A Cryogenian chronology: Two long-lasting synchronous Neoproterozoic glaciations. Geology, 43(5), 459-462.

Rose, C. V., Swanson-Hysell, N. L., Husson, J. M., Poppick, L. N., Cottle, J. M., Schoene, B., & Maloof, A. C. (2012). Constraints on the origin and relative timing of the Trezona δ13C anomaly below the end-Cryogenian glaciation. Earth and Planetary Science Letters, 319, 241-250.

Strauss, J. V., MacDonald, F. A., Halverson, G. P., Tosca, N. J., Schrag, D. P., & Knoll, A. H. (2015). Stratigraphic evolution of the Neoproterozoic Callison Lake Formation: Linking the

break-up of Rodinia to the Islay carbon isotope excursion. American Journal of Science, 315(10), 881-944.

Sumner, D.Y., Jungblut, A., Hawes, I., Andersen, D., Mackey, T., & Wall, K. (2016). Growth of elaborate microbial pinnacles in Lake Vanda, Antarctica. Geobiology, 14(6), 556-574.

Sumner, D.Y. (1997). Late Archean calcite-microbe interactions; two morphologically distinct microbial communities that affected calcite nucleation differently. Palaios, 12(4), 302-318.

Suosaari, E. P., Reid, R. P., Oehlert, A. M., Playford, P. E., Steffensen, C. K., Andres, M. S., . . . Eberli, G. P. (2019). Stromatolite provinces of Hamelin Pool: Physiographic controls on stromatolites and associated lithofacies. Journal of Sedimentary Research, 89(3), 207-226.

Sztanó, O. (1995). Palaeogeographic significance of tidal deposits: an example from an early Miocene Paratethys embayment, northern Hungary. Palaeogeography. Palaeoclimate Palaeoecology, 113, 173-187.

Truswell, J., & Eriksson, K. (1973). Stromatolitic associations and their palaeo-environmental significance: a re-appraisal of a Lower Proterozoic locality from the northern Cape Province, South Africa. Sedimentary Geology, 10(1), 1-23.

Visscher, P. T., Reid, R. P., & Bebout, B. M. (2000). Microscale observations of sulfate reduction: correlation of microbial activity with lithified micritic laminae in modern marine stromatolites. Geology, 28(10), 919-922.

Vlasov, F. Ya., 1977, Dokembriyskie stromatolity iz satkinskpy svity yuzhnogo Urala, in Materialy po paleontologii srednego paleozoya Urala

i Sibirii. (Precambrian stromatolites from the Satka Formation of the Southern Urals.): Sverdlovsk. Akademiya Nauk SSSR, Uralskiy Nauchnyy Tzentr, Trudy Instituta Geologii i Geokhimii, 128, 101-128.

Wallace, M. W., Hood, A.V.S., Fayle, J., Hordern, E. S., & O'Hare, T. F. (2019). Neoproterozoic marine dolomite hardgrounds and their relationship to cap dolomites. Precambrian Research, 328, 269-286.

Wallace, M. W., vS Hood, A., Woon, E. M., Giddings, J. A., & Fromhold, T. A. (2015). The Cryogenian Balcanoona reef complexes of the Northern Flinders Ranges: implications for Neoproterozoic ocean chemistry. Palaeogeography, Palaeoclimatology, Palaeoecology, 417, 320-336.

Walker, R. G. P., Plint, A.G. (1992). Wave and storm dominated shallow marine systems. Facies Models-response to sea level change-, 219-238.

Walter, M. R. (1976). Stromatolites: Elsevier. New York: Elsevier. 1-790.

FIGURE CAPTIONS

Figure 1. Geological map of Neoproterozoic strata near Blinman, Central Flinders Ranges, South Australia. Modified from the Parachilna Region geological map (compiled by Reid and Preiss, 1999).

Figure 2. Generalized stratigraphy of the Neoproterozoic Umberatana Group in the central Flinders Ranges, South Australia. Modified from Preiss et al., 1987.

Figure 3. Measured sections and interpreted correlations (note: faulting does not allow for precise correlation, see Fig. 1). Note relative abundance of carbonate facies in the south at Bulls Gap (left), and increase in mudstone in the northern sections, Angorichina and Glass Gorge (right). Measured section localities (Bulls Gap, Angorichina Hostel, Angorichina Station, and Glass Gorge Road) are shown in Fig. 1.

Figure 4. Field photos of the Enorama Shale. A. Red mudstone with thin silty beds transitioning upwards into the Trezona Formation. Angorichina Hostel. B. Mudstone interbedded with sharp-based sands with hummocky cross stratification; a potential storm event bed, Angorichina Hostel. C. Flute casts from the underside of silty beds of the Enorama Shale, Glass Gorge. Paleocurrents (when in place) are oriented north. D. Scoured bed with climbing ripples, possibly a sandy turbidite, Angorichina Hostel.

Figure 5. Field photographs of the lower siliciclastic member, Trezona Formation. A. Mudstone at base transitions upwards to poorly sorted intraclastic packstone, calcareous mudstone, hardgrounds (arrow), an irregular erosion surface, and then a resistant deep water stromatolite horizon. Stromatolites are overlain by mudstone. B. Cross section view of cuspate stromatolites, Angorichina Hostel C. Elongate poorly-sorted intraclastic packstone with an erosional base. Note possible hardground at top of bed, Angorichina Hostel. D. Irregular erosion surface overlain by poorly-sorted intraclastic packstone (in topographic lows, arrow a) and cuspate stromatolites (topographic highs, arrow c). Note truncation of red mudstone beds by the erosion surface (arrow b), Angorichina Hostel.

Figure 6. Idealized deep water cycle in the lower siliciclastic member. Transgression, regression, and relative sea level change do not suppose a driving mechanism (e.g., subsidence, eustacy, sediment supply).

Figure 7. Field photographs of the upper siliciclastic member, Trezona Formation. A. Iron-rich rounded and elongate intraclasts, Angorichina Station. B. Bidirectional crossbedding in intraclast grainstone, Emu Gap. C. Crossbedded fine-grained grainstone with mud-drapes. Note wavy, flaser, and lenticular bedding at the base of the crossbedded grainstone, Angorichina Hostel D. Domal stromatolites in plan view, Glass Gorge. D. Wavy, flaser and lenticular bedding, Angorichina Hostel. E. Regular cyclicity in the siliciclastic member, north of Bulls Gap.

Figure 8. Upper carbonate member of the Trezona Formation. A. Contact between the siliciclastic member and the carbonate member (arrow). Note change in vegetation at the contact.

Fine-grained carbonate at base of the carbonate member grades up into massive carbonate beds at the top of the Trezona Formation. B. Rounded intraclastic grainstone bed overlain by columnar stromatolites. C. Longitudinal stromatolites oriented N-NW, Bulls Gap. D. Desiccation-cracked red calcareous mudstone, Bulls Gap. E. Blue oolitic grainstone, Angorichina Station. F. Thin section photomicrograph of iron-rich giant ooids, Bulls Gap. Note alternating iron-rich laminae (red) and micritic laminae (grey).

Figure 9. Cuspate stromatolites in the Trezona Formation. A–B. Deep-water cuspate stromatolite horizons overlying an erosion surface, Angorichina Hostel. (north to the right of the images). Arrow in B points to intraclasts in topographic lows of the erosion surface. C. Macrostructure of elongate cuspate stromatolite domes in plan view, Emu Gap. Note cusp ridge lines oriented perpendicular to elongation direction. D. Plan view of cuspate ridges on stromatolite dome oriented perpendicular to paleo downslope direction. E. Cross section of cuspate stromatolite laminae with stacked cusp peaks drifting to the north (right). F. Line drawing of cuspate stromatolites. G. Field sketch and interpretation of cuspate stromatolites at Bulls Gap.

Figure 10. Thin section photo-micrographs of cuspate stromatolite microstructure. A. Interlaminated dark micritic carbonate, light micritic carbonate, and stylolitized dark red laminae. B. Dark micritic cuspate lamina (arrow). Note fine grained disseminated hematite. C. Interlaminated dark micritic and light micritic carbonate, and stylolitized dark red laminae. D. Upward branching shrubby micritic microbial textures (arrow). Inter-microbial space is filled with microspar.

Figure 11. A comparison of some Precambrian cuspate stromatolites and microbialites. A. Cuspate stromatolites from the Cryogenian Umberatana Group, Trezona Formation. B. Cuspate stromatolites from slope facies of the Paleoproterozoic Pethei Group. C. Cuspate stromatolites from the Archean Campbellrand Subgroup, Gamohaan Formation, coin is 16 mm diameter. D. Cuspate stromatolites from the Neoproterozoic Mount Harper Group, Callison Lake Formation.

Table 1. Lithology and Interpretation

Formation	Member		Lithology/Facies	Process Interpretation	Environmental Interpretation
Enorama Shale			Mudstone, rare silty-sandy beds with flute casts, rare sharp bedded silty-sandy beds with parallel lamination overlain by hummocky rippled beds	Low energy deposition with rare turbidites and storm beds.	Deep water basinal to outer ramp. Below fwwb, some intervals above swb
Trezona Formation	siliciclastic member	lower	Calcareous mudstone	Sediment starved low energy deposition. Hardgrounds. Authigenic precipitation of dolomite on the seafloor (Wallace et al., 2019)	outer ramp
			Erosively-based, poorly sorted platy intraclastic packstone with chaotic arrangement of clasts. Can be capped with hardground.	Debris flow	outer ramp
			Erosion surfaces. Often capped by hardground.	Marine erosion, possibly associated with debris flows on ramp and/or strong erosional currents. Associated with extreme sediment starvation.	outer ramp
			Elongate cuspate stromatolites	Sediment starved, deep water microbial carbonate deposition. Condensed deposition. Maximum transgression	outer ramp (where best developed)
			Mudstone	Deep water low energy suspension settling	mid-outer ramp
			Mudstone and siltstone with flute casts, unidirectional and climbing ripples	Turbidites, storm event beds(?)	mid-outer ramp
			Erosively-based, poorly-moderately sorted platy intraclastic packstone with edgewise and imbricated fabrics. Can be capped with a hummocky fine-grained grainstone. Rare.	Storm event bed or storm reworking of debris flow	mid ramp
		upper	Domal, columnar, and elongate cuspate stromatolites	Microbial carbonate deposition during intervals of sediment starvation	mid ramp
			Rare erosion surfaces. Not capped with hardground.	Marine erosion via strong currents, and/or mass wasting on ramp	mid ramp
			Mudstone	Low energy suspension settling	mid-inner ramp
			Rounded, crossbedded intraclastic packstone-grainstone and fine-grained grainstone. Mud-drapes, bidirectional paleocurrents, some channelization.	Wave and tide-worked bedforms. Some tidal bars, tidal channels. Shallow water equivalents of debris flows offshore(?). Subtidal	inner ramp, tidal channels possibly mid-inner ramp(?)
			Wavy, flaser, and lenticular heterolithic bedding (mud to v.fg. sand mixed lithologies)	Reworking and deposition by tidal currents. Subtidal.	inner ramp
	carbonate member		Calcareous mudstone	Low energy suspension settling	mid-inner ramp(?) (similar environment to upper siliciclastic member but more

		carbonate rich)
Low relief, longitudinal, and columnar stromatolites. Very rare elongate cuspate stromatolites	Microbial carbonate deposition during intervals of sediment starvation	mid-inner ramp(?) (similar environment to upper siliciclastic member but more carbonate rich)
Rounded and well-sorted intraclastic grainstone	Wave-worked intraclasts	inner ramp
Ooid grainstone. Giant ooids. Giant ooids with iron oxide rich laminae.	Continuous agitation of sediment in shallow, high energy conditions. Extremely high carbonate supersaturation (giant ooids). Fluctuating redox conditions (micrite and iron oxide rich laminae)	inner ramp
Domal and columnar stromatolite bioherms	Shallow marine microbial carbonate deposition	inner ramp

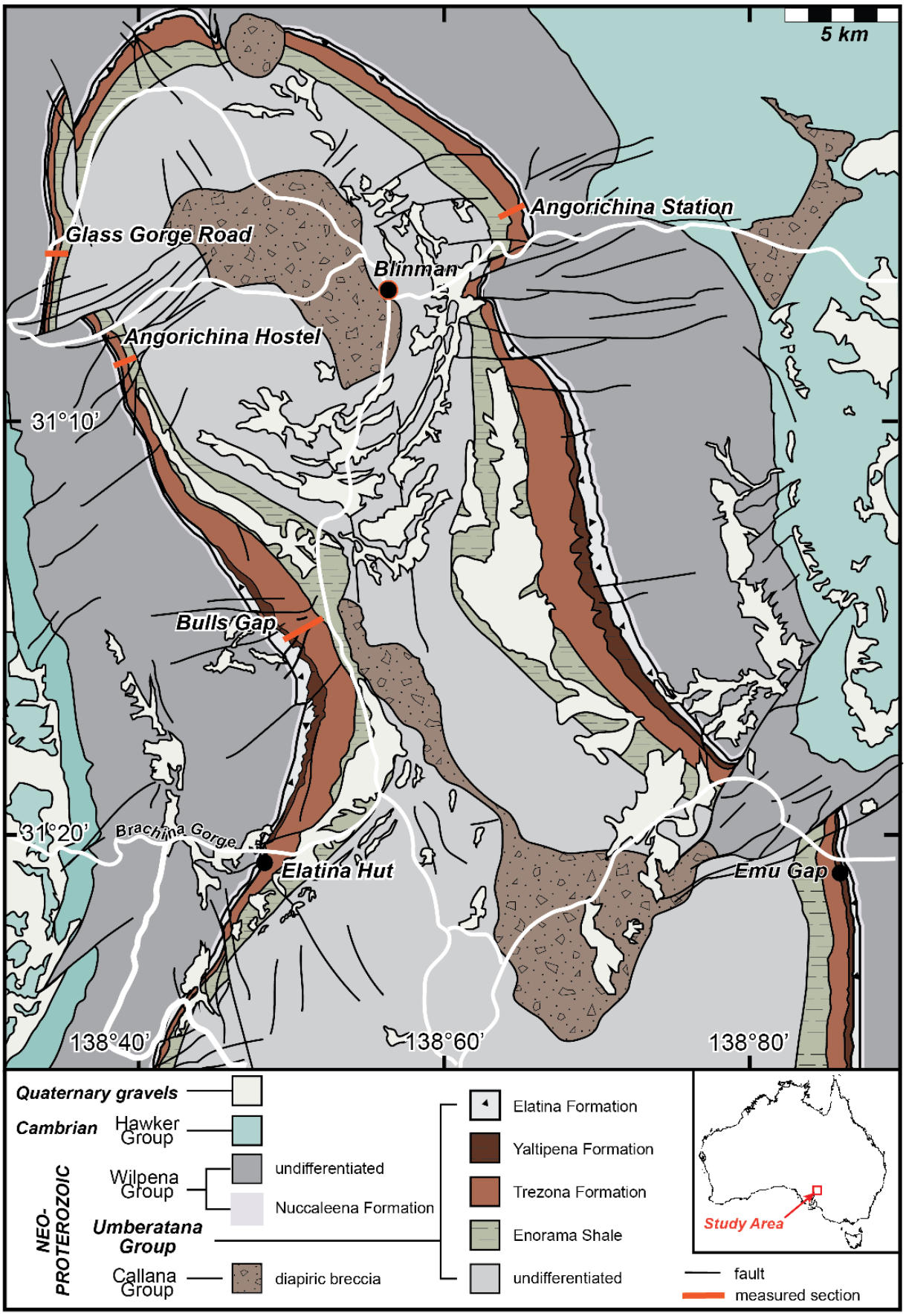

gbi_12479_f1.png

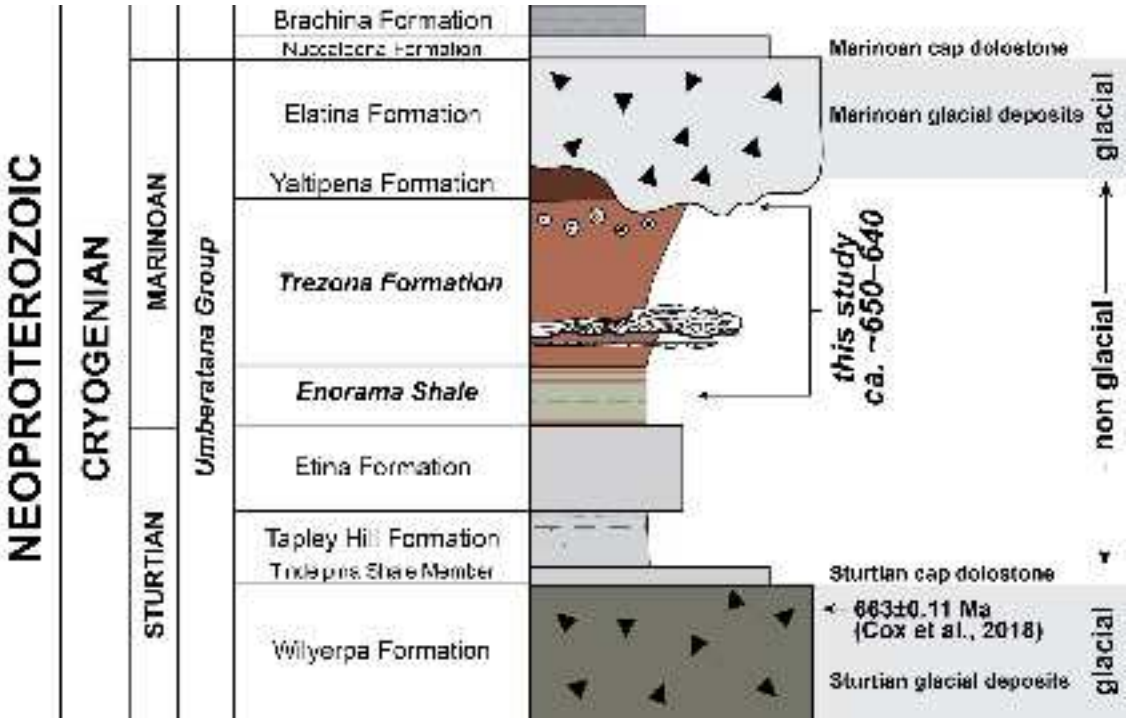

gbi_12479_f2.png

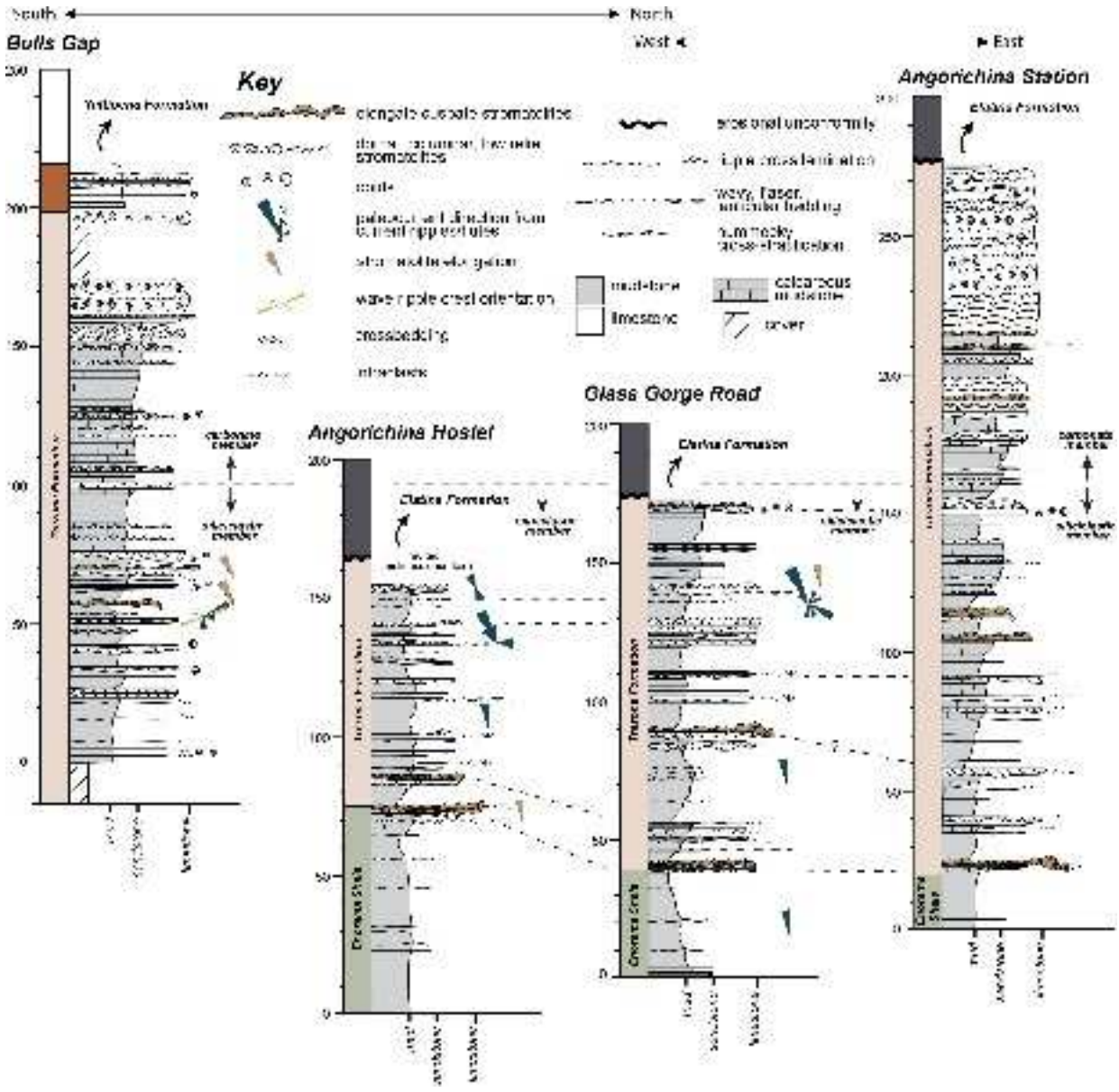

gbi_12479_f3.png

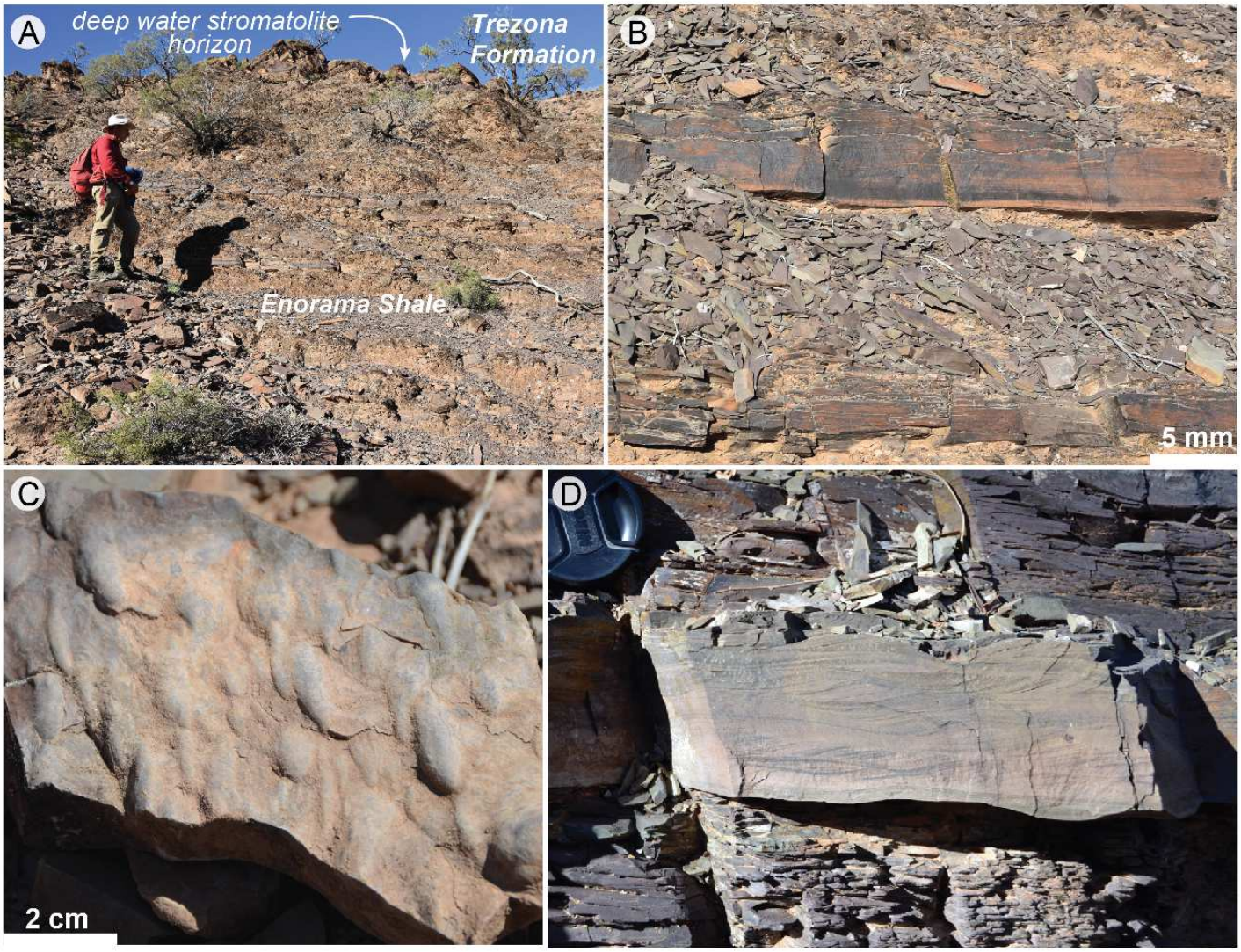

gbi_12479_f4.png

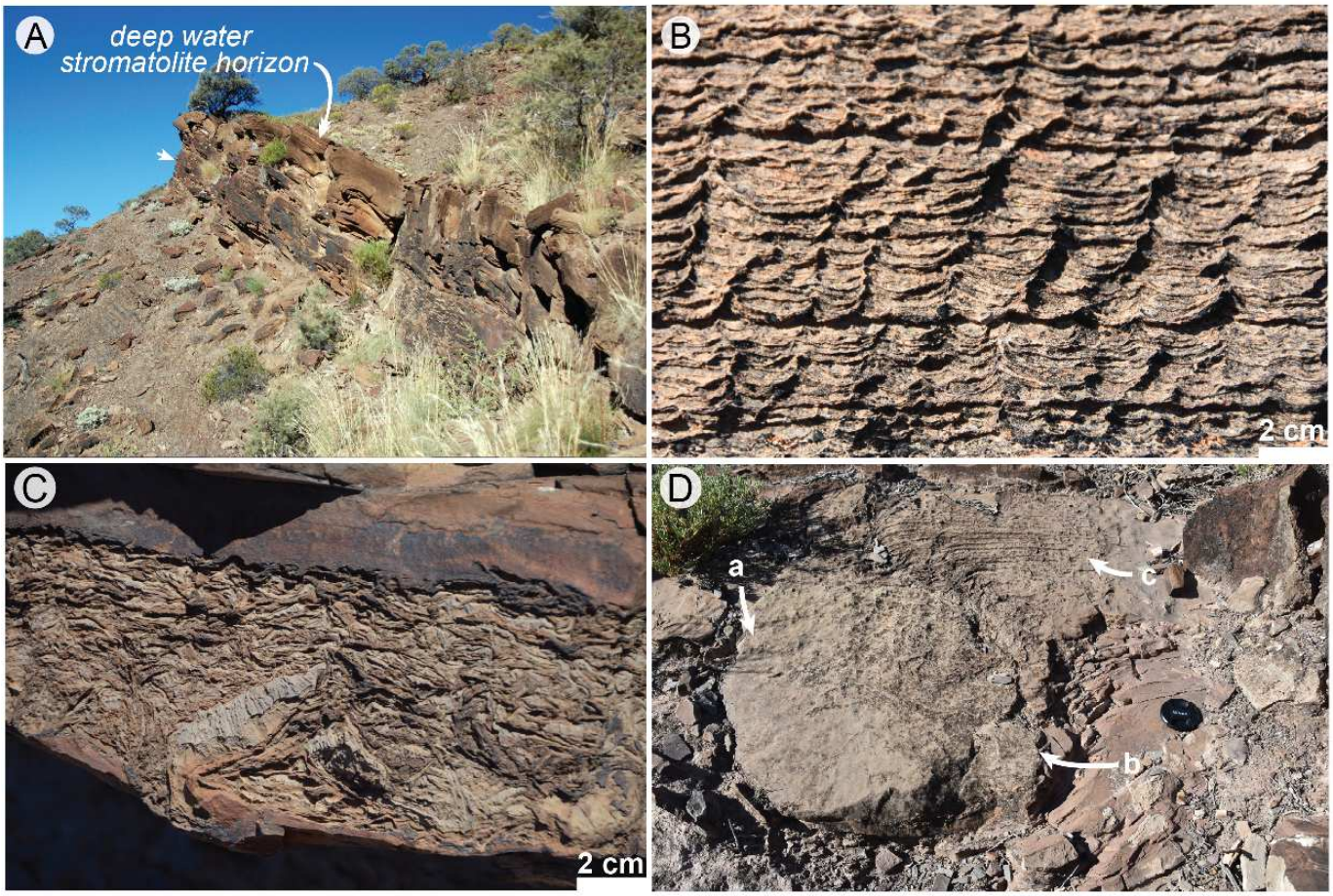

gbi_12479_f5.png

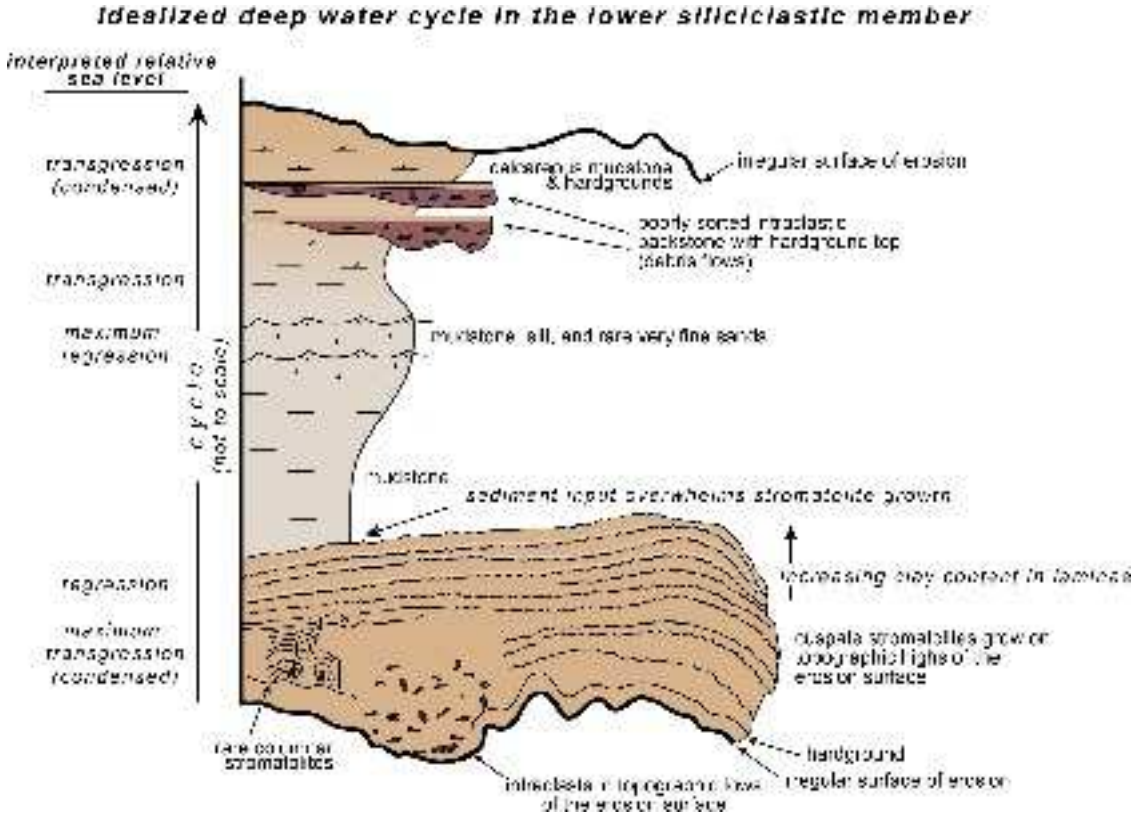

gbi_12479_f6.png

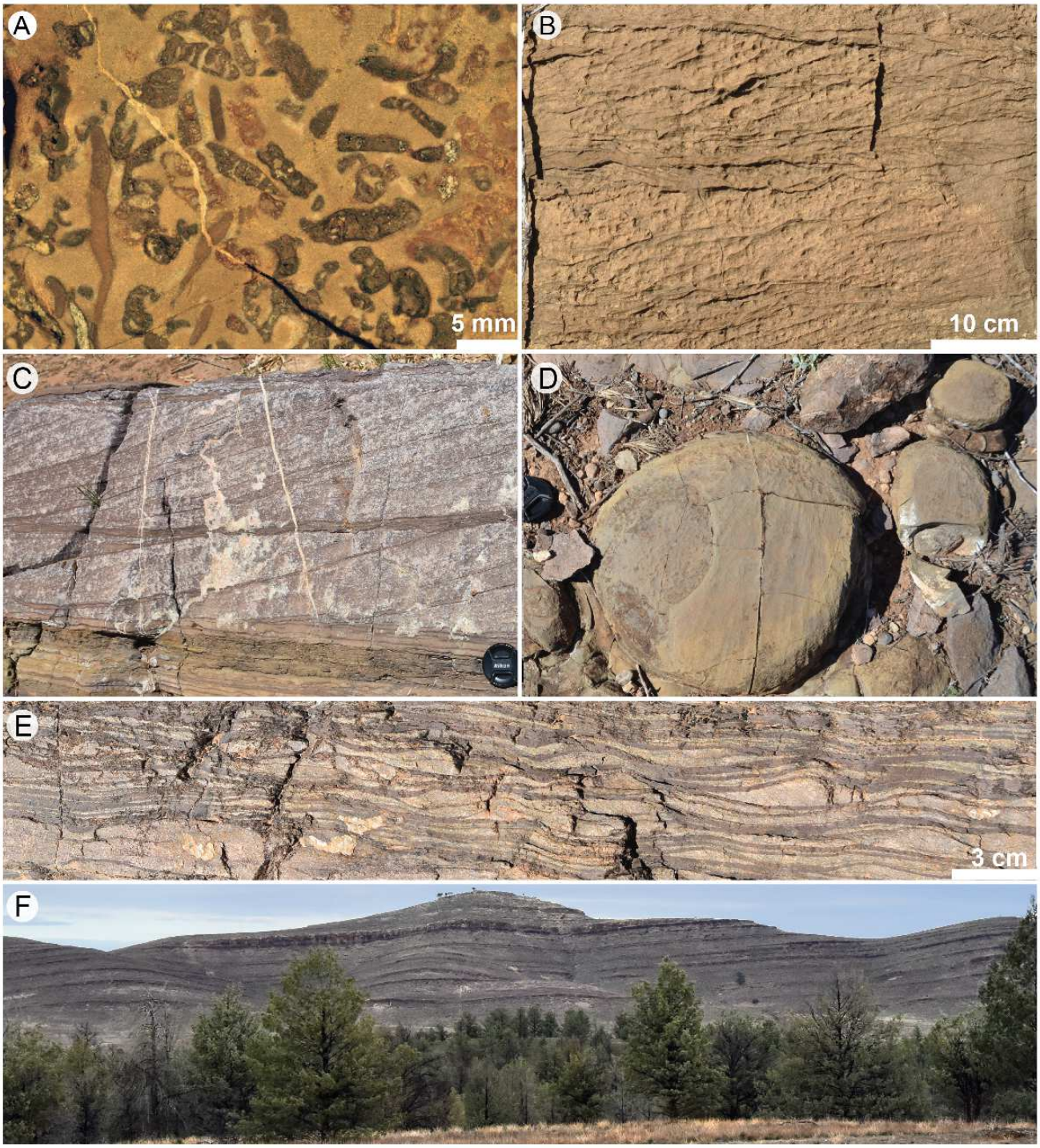

gbi_12479_f7.png

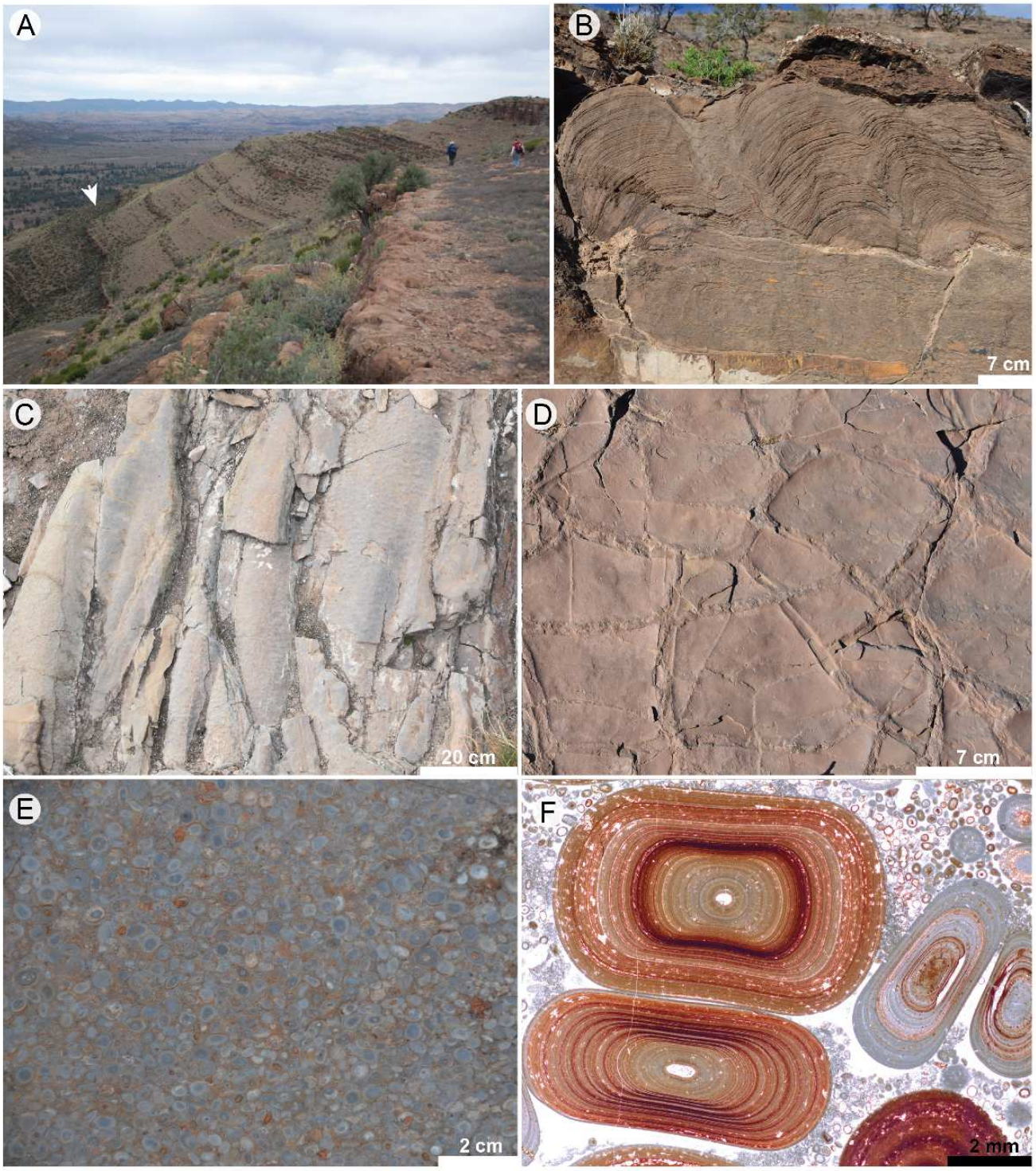

gbi_12479_f8.png

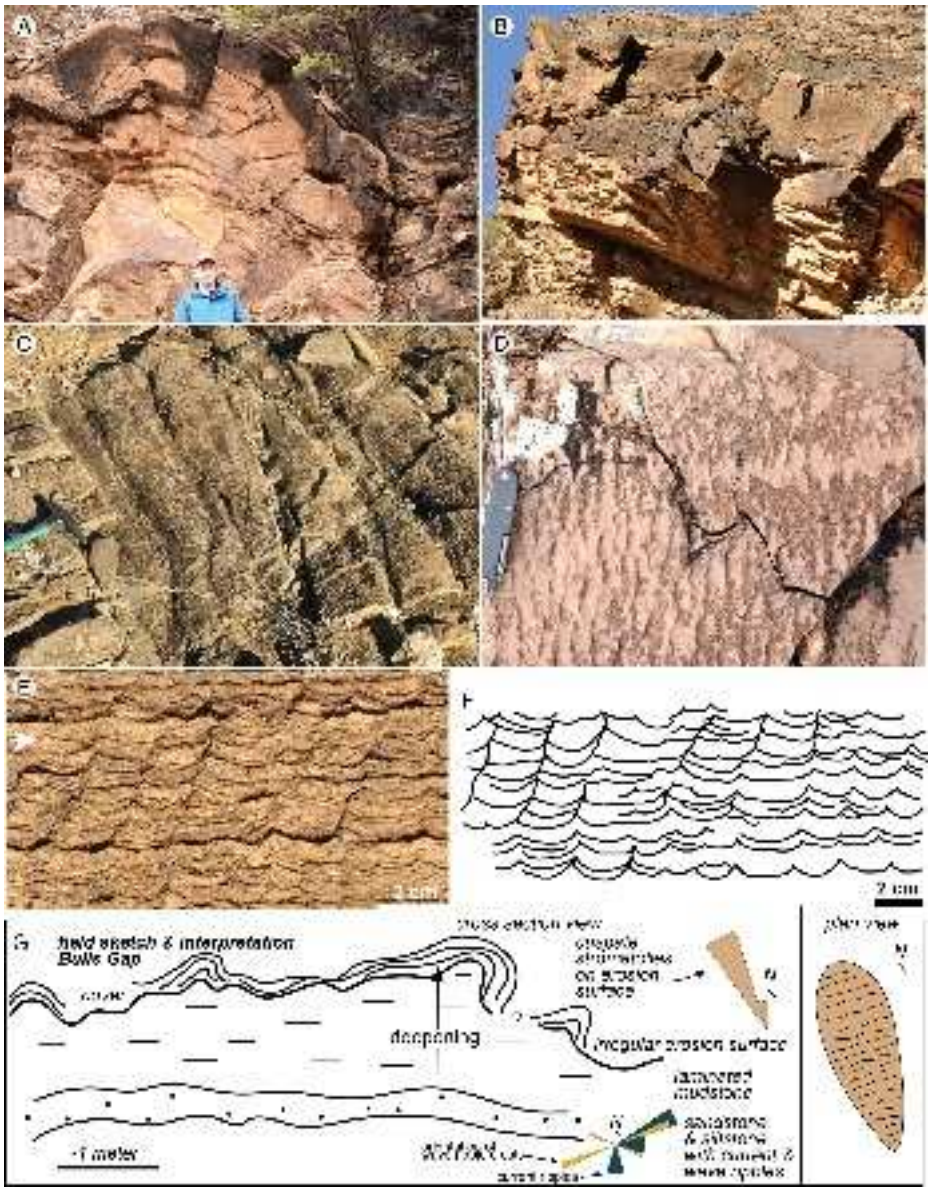

gbi_12479_f9.png

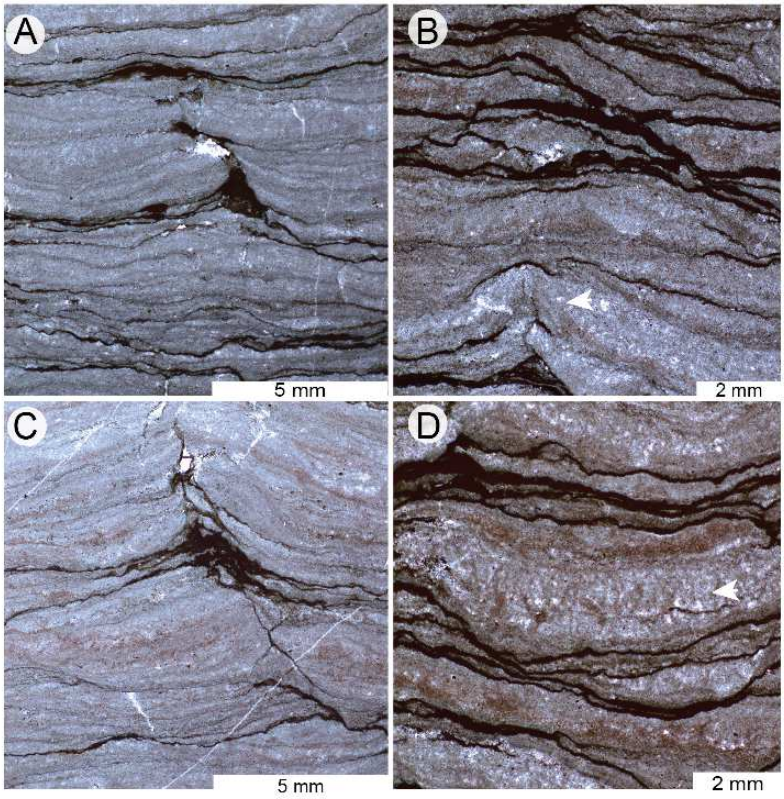

gbi_12479_f10.png

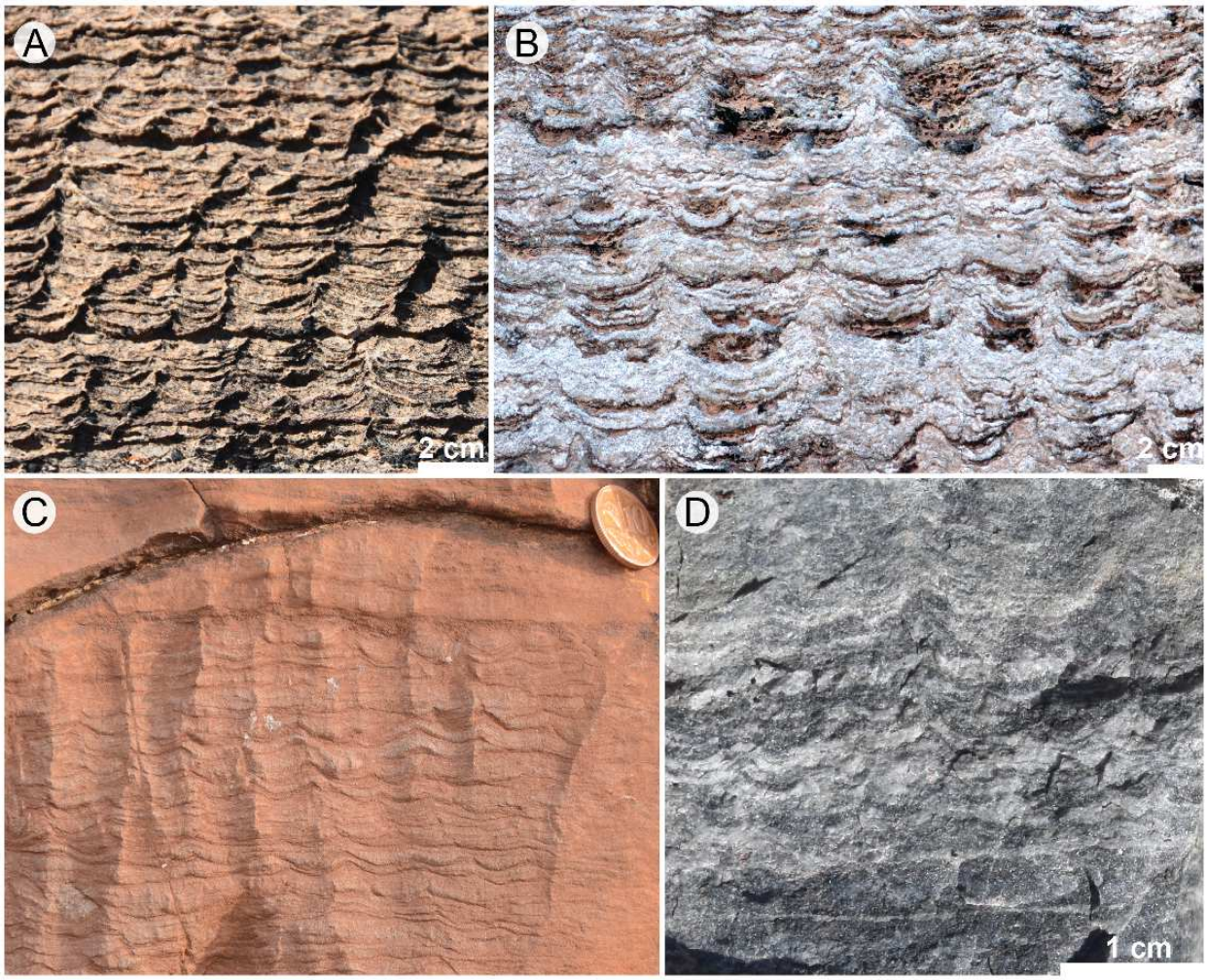

gbi_12479_f11.png